AGU PUBLICATIONS

JGR

Journal of Geophysical Research: Solid Earth

RESEARCH ARTICLE
10.1002/2014JB011660

Key Points:
- Spine extrusion is associated with cyclic seismicity
- Frictional melting is achieved over a power density of 0.3 MW m^{-2}
- Frictional melting influences slip dynamics

Supporting Information:
- Figures S1 and S2

Correspondence to:
A. J. Hornby,
a.hornby@liverpool.ac.uk

Citation:
Hornby, A. J., et al. (2015), Spine growth and seismogenic faulting at Mt. Unzen, Japan, *J. Geophys. Res. Solid Earth*, *120*, doi:10.1002/2014JB011660.

Received 4 OCT 2014
Accepted 27 APR 2015
Accepted article online 29 APR 2015

©2015. American Geophysical Union. All Rights Reserved.

Spine growth and seismogenic faulting at Mt. Unzen, Japan

Adrian J. Hornby[1], Jackie E. Kendrick[1], Oliver D. Lamb[1], Takehiro Hirose[2], Silvio De Angelis[1], Felix W. von Aulock[1], Kodo Umakoshi[3], Takahiro Miwa[4], Sarah Henton De Angelis[1], Fabian B. Wadsworth[1,5], Kai-Uwe Hess[5], Donald B. Dingwell[5], and Yan Lavallée[1]

[1]Earth, Ocean and Ecological Sciences, University of Liverpool, Liverpool, UK, [2]Kochi Institute for Core Sample Research (KCC), JAMSTEC, Kochi, Nankoku, Japan, [3]Graduate School of Fisheries Science and Environmental Studies, Nagasaki University, Nagasaki, Japan, [4]National Research Institute for Earth Science and Disaster Prevention, Ibaraki, Japan, [5]Department for Earth and Environmental Science, Ludwig Maximilian University, Munich, Germany

Abstract The concluding episode of activity during the recent eruption of Mt. Unzen (October 1994 to February 1995) was characterized by incremental spine extrusion, accompanied by seismicity. Analysis of the seismic record reveals the occurrence of two dominant long-period event families associated with a repeating, nondestructive source mechanism, which we attribute to magma failure and fault-controlled ascent. We obtain constraints on the slip rate and distance of faulting events within these families. That analysis is complemented by an experimental thermomechanical investigation of fault friction in Mt. Unzen dacitic dome rock using a rotary-shear apparatus at variable slip rates and normal stresses. A power density threshold is found at 0.3 MW m^{-2}, above which frictional melt forms and controls the shear resistance to slip, inducing a deviation from Byerlee's frictional law. Homogenized experimentally generated pseudotachylytes have a similar final chemistry, thickness, and crystal content, facilitating the construction of a rheological model for particle suspensions. This is compared to the viscosity constrained from the experimental data, to assess the viscous control on fault dynamics. The onset of frictional melt formation during spine growth is constrained to depths below 300 m for an average slip event. This combination of experimental data, viscosity modeling, and seismic analysis offers a new description of material response during conduit plug flow and spine growth, showing that volcanic pseudotachylyte may commonly form and modify fault friction during faulting of dome rock. This model furthers our understanding of faulting and seismicity during lava dome formation and is applicable to other eruption modes.

1. Introduction

Lava dome eruptions are one of the most hazardous forms of volcanic activity. Dome destabilization may generate block-and-ash flows as well as catastrophic explosive eruptions. Magma ascent during dome eruptions has been described as cyclic at timescales of seconds to years [*Voight*, 1999; *Sparks*, 2000; *Harris et al.*, 2003; *Costa et al.*, 2013; *Lamb et al.*, 2014], where longer timescales are attributed to variations in the magmatic system and shorter timescales are generally believed to reflect shallow conduit processes, including the rheological stability of magma. Careful monitoring of lava domes is thus central to mitigating the risk posed by their activity. Seismic monitoring in particular has revealed that magma transport in dome-building eruptions is a rich source of earthquakes, and analysis has revealed the importance of discerning the frequency and period of earthquakes emanating from the uppermost (<3 km) edifice [*Chouet and Matoza*, 2013]. Many studies have attempted to describe the source mechanisms underlying these signals: high-frequency and hybrid seismic signals have been interpreted to originate from magma fracturing processes [*Harrington and Brodsky*, 2007; *De Angelis and Henton*, 2011; *Umakoshi et al.*, 2011], while shallow long-period (LP) seismicity has been associated with resonance of fluid in the conduit [*Neuberg et al.*, 2006; *Thomas and Neuberg*, 2012], or in a crack [*Chouet*, 1988; *Burlini et al.*, 2007; *Benson et al.*, 2008; *Maryanto et al.*, 2008]. A recent study, employing proximal seismometer networks, has proposed that LP events may also be caused by slow rupture of weak volcanic materials [*Bean et al.*, 2013].

Lava dome eruptions at Mt. Unzen (Japan), Mount St. Helens (USA), Soufrière Hills volcano (Montserrat), Volcán De Colima (Mexico), and Santiaguito dome complex (Guatemala) have all been characterized by cyclic behavior [*Iverson et al.*, 2006; *Neuberg et al.*, 2006; *Umakoshi et al.*, 2008; *Johnson et al.*, 2014; *Lamb et al.*, 2014]. The seismic signals emitted contain a characteristic sequence of waveform families with event counts that emerge and

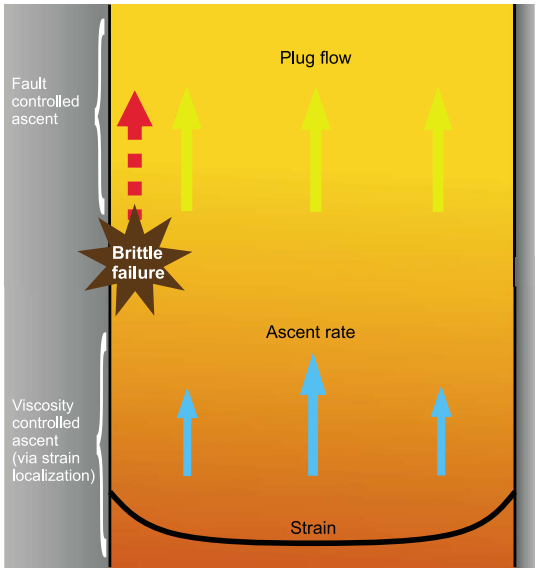

Figure 1. Conceptual model of magma ascent within a shallow conduit cross section. Arrows represent relative magma ascent rate across the conduit. Strain localization of viscously ascending magma at the conduit walls is shown in the lower half of the figure as friction inhibits flow at the conduit walls, localizing strain. This may force magma to fail, and slip can occur near the conduit walls, causing a transition from viscosity- to fault-controlled ascent as illustrated in the center of the figure. Above this point, magma moves as a solid plug and slip dynamics are governed by friction along the slip interface.

decay in a near-sinusoidal fashion, simultaneous with cycles of tilt. Seismic output often increases during inflation and decreases following rapid deflation, once a threshold is reached, after which the cycles begin again [e.g., *Neuberg et al.*, 2006]. The threshold in question has been modeled to reflect friction along faults that form at the conduit margin as magma releases the stress accumulated during inflation by fracturing, leading to the pulsatory extrusion of spines [*Iverson et al.*, 2006; *Neuberg et al.*, 2006; *Lensky et al.*, 2008; *Massol and Jaupart*, 2009; *Scharff et al.*, 2014]. Spines are dense, degassed, and high-viscosity magma plugs, extruded as coherent bodies bounded by marginal fault zones [*Cashman et al.*, 2008; *Pallister et al.*, 2013]. Gas pressurization beneath the plug has commonly been cited as the driving force for fracture propagation [*Voight*, 1999; *Johnson et al.*, 2008; *Massol and Jaupart*, 2009; *Lyons et al.*, 2012], and the mechanical contributions from magma failure and slip events [*Lavallée et al.*, 2011; *Thomas and Neuberg*, 2012; *Chouet and Matoza*, 2013; *Kendrick et al.*, 2014a], outgassing pulses [*Voight*, 1999; *Waite et al.*, 2008; *Massol and Jaupart*, 2009; *Collinson and Neuberg*, 2012; *Michaut et al.*, 2013], and wall rock elasticity [*Costa et al.*, 2007, 2012] have been proposed to contribute to short-term cyclicity in monitored geophysical and geochemical signals.

Evidence from field, experimental, and numerical studies show that strain localization in magmas can control ascent dynamics in a volcanic conduit. During ascent, magma undergoing localized strain near the conduit margin may yield to brittle failure [*Yamasato*, 1998; *Goto*, 1999; *Tuffen and Dingwell*, 2004; *Lensky et al.*, 2008; *De Angelis and Henton*, 2011; *Okumura et al.*, 2013] and slip [*Thomas and Neuberg*, 2012; *Lavallée et al.*, 2013; *Kendrick et al.*, 2014a]. Rheologically, the presence of multiple phases in magma (liquids, crystals, and gas bubbles) partitions the applied stress, and as strain rate across a conduit of ascending magma varies nonlinearly, shear thinning favors strain localization at the conduit margin [*Caricchi et al.*, 2007; *Lavallée et al.*, 2013; *Okumura et al.*, 2013]. Extensive strain and high strain rates in this area may lead to seismogenic magma failure [*Lavallée et al.*, 2008; *Cordonnier et al.*, 2009], marking the onset of friction-controlled ascent [*Kendrick et al.*, 2014a]. These two scenarios for magma ascent are illustrated in the upper and lower parts of the conceptual model in Figure 1.

The processes and criteria attendant on magma failure have been the subject of several experimental [*Alidibirov and Dingwell*, 1996; *Dingwell*, 1996; *Gonnermann and Manga*, 2003; *Rust et al.*, 2004; *Spieler et al.*, 2004; *Okumura et al.*, 2010; *Lavallée et al.*, 2011; *Cordonnier et al.*, 2012a; *Costa et al.*, 2012] and numerical [*Costa et al.*, 2007; *Hale and Wadge*, 2008; *Collinson and Neuberg*, 2012] studies, but knowledge of the frictional properties of volcanic fault rocks is more scarce [*Moore et al.*, 2008; *Kennedy et al.*, 2009; *Lavallée et al.*, 2012, 2014; *Kendrick et al.*, 2014b; *Violay et al.*, 2014]; thus, our ability to interpret the geophysical signals that accompany volcanic unrest remains insufficient.

1.1. Fault Friction

The process of fault slip has been extensively studied in earthquake physics in past decades [*Sibson*, 1975; *Spray*, 1992; *Tsutsumi and Shimamoto*, 1997; *Di Toro et al.*, 2006a; *Beeler et al.*, 2008; *Faulkner et al.*, 2011; *Chang et al.*, 2012; *Hirose et al.*, 2012]. At low slip velocities, rock friction observations have led to the conception of rate- and state-dependent friction laws [*Dieterich*, 1978; *Ruina*, 1983; *Dieterich and Kilgore*,

1994], and for normal stress <200 MPa (i.e., shallow crustal conditions), the relationship between shear stress (τ) and normal stress (σ_n) is well described by Byerlee's empirical friction law [*Byerlee*, 1978]:

$$\tau = 0.85\sigma_n \quad (1)$$

At high slip velocities, however, the shear resistance to slip exhibits a strong departure from this relationship, which has generally been attributed to flash heating due to the conversion of mechanical work into heat [*Spray*, 1992; *Goldsby and Tullis*, 2011]. Slip at high power densities (the product of slip rate and shear stress) may generate sufficient heat to induce frictional melting in silicate rocks—a process preserved in the geologic record in the form of pseudotachylyte [*Shand*, 1916; *Sibson*, 1975]. In cases where a fault hosts gouge material, mineral decomposition and strain localization at high slip rate have also been shown to provide low friction coefficients [*Mizoguchi et al.*, 2009; *Di Toro et al.*, 2011; *Hirose et al.*, 2012; *Lavallée et al.*, 2014].

Friction in volcanic conduits and during spine extrusion is especially important for the final stage of magma ascent in the uppermost ~1–2 km [*Kennedy et al.*, 2009; *Pallister et al.*, 2013] and shows a dependence on velocity and normal stress. Experiments have shown that failure, followed by slip at low power density, engenders comminution and cataclastic ash generation [*Kennedy and Russell*, 2012]. Ascent mechanics of the spine may be influenced by incorporation of fragmented ash and breccia in the fault surface at shallow depths due to low normal stresses [*Kendrick et al.*, 2012]. The frictional properties of volcanic ash have been experimentally determined at low to high slip velocities. At low slip rate (10^{-6}–10^{-3} m s^{-1}), faults bearing volcanic ash gouge change from rate weakening to rate strengthening [*Moore et al.*, 2008] and exhibit strain hardening [*Kennedy and Russell*, 2012]. A recent study of high-velocity rotary shear (HVR) experiments on volcanic ash gouge from different volcanoes (including Mt. Unzen) has extended the description of ash gouge friction (at ambient temperature), providing a frictional law to constrain rate-weakening behavior at a range of slip velocities of up to 1.3 m s^{-1} and normal stresses of up to 2.5 MPa [*Lavallée et al.*, 2014]. In ash gouge experiments, high temperatures may be achieved, possibly prompting rapid viscous sintering, which raises the question of the longevity of (particulate) volcanic ash in conduit slip zones [*Bizzarri*, 2014; *Kolzenburg and Russell*, 2014].

Field and experimental evidence has suggested that faulting during dome eruptions may commonly result in frictional melting even over short slip distances, owing to the high temperatures (and low fusion temperatures) of dome lavas in the magmatic column [*Kendrick et al.*, 2014a, 2014b]. Rotary shear experiments have helped shape our understanding of frictional melt and its rheology and role during energetic seismogenic faulting. At high slip rates, rapid and intense heat generation achieves temperatures in excess of the fusion temperature of some, or all of the mineral phases, to form a melt [*Shimamoto and Lin*, 1994; *Di Toro et al.*, 2006a; *Spray*, 2010]. The rheology of silicate melts is very well described in terms of composition, temperature, and strain rate [*Webb and Dingwell*, 1990; *Dingwell et al.*, 1996; *Hess and Dingwell*, 1996; *Hess et al.*, 1996a, 1996b; *Giordano et al.*, 2008], and, to some extent, in terms of crystal and vesicle fraction [*Lejeune et al.*, 1999; *Caricchi et al.*, 2007; *Lavallée et al.*, 2007; *Cimarelli et al.*, 2011; *Mueller et al.*, 2011; *Cordonnier et al.*, 2012a; *Mader et al.*, 2013; *Truby et al.*, 2015]; yet its control on fault friction has received little attention [*Bowden and Persson*, 1961; *Spray*, 1993; *Fialko and Khazan*, 2005; *Nielsen et al.*, 2008; *Sone and Shimamoto*, 2009; *Violay et al.*, 2014]. *Lavallée et al.* [2012] stated that volcanic frictional melts have a non-Arrhenian temperature-dependent viscosity and, at volcanically relevant strain rates, display a small component of shear thinning behavior. Under tectonic conditions, it has been observed that frictional melt lubricates the fault plane [*Spray*, 2005; *Di Toro et al.*, 2006a, 2011; *Brown and Fialko*, 2012]; however, studies have revealed high shear resistances induced by the presence of frictional melt at low normal stresses that suggest they may act as an adhesive (or viscous brake) to slip [*Fialko*, 2004; *Koizumi et al.*, 2004]. This is particularly important in shallow volcanic settings where it provides an additional rheological contribution to fault slip instability and may help control the stick-slip phenomenon that produces drumbeat seismicity during magma ascent [*Kendrick et al.*, 2014a]. The significance of frictional melting in shallow volcanic processes requires further study. Here we have expanded and constrained the application of frictional properties to lava dome eruptions by combining seismic analysis, experiments, and rheological modeling to evaluate the role of fault processes during spine extrusion in 1994–1995 at Mt. Unzen.

1.2. Spine Growth at Mt. Unzen

Mt. Unzen underwent a protracted period of dome growth between 1991 and 1995 [*Nakada et al.*, 1999]. In less than 4 years, 2.1×10^8 m^3 of magma (dense rock equivalent) was erupted at discharge rates of

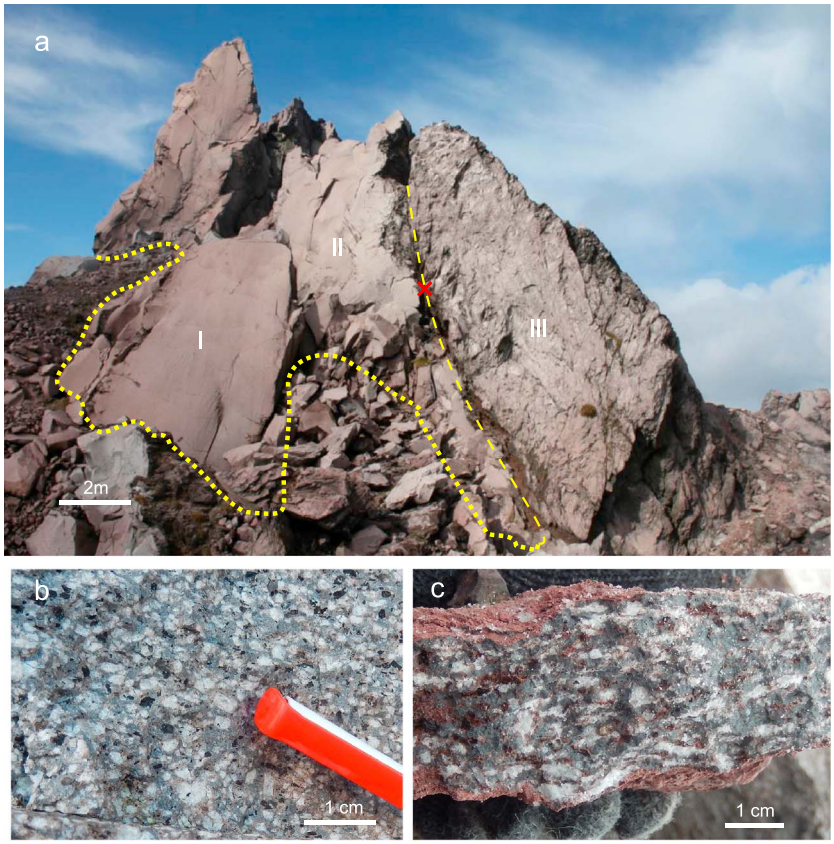

Figure 2. (a) The relict 1994–95 spine at Mt. Unzen volcano, showing a range of deformation types, including (I) a viscously sheared spine interior showing cavitation structures [*Smith et al.*, 2001] and grading of macroscopic fractures increasing in number toward (II) an intensely sheared block showing the textural record of viscous to brittle deformation bounded to the right by the core of the fault zone (dashed line) and (III) fault breccia consisting of large blocks and sintered fragmented ash and gouge which has become welded to and extruded with the spine. (b) Undeformed rock specimen from Mt. Unzen dome, showing large euhedral phenocrysts of plagioclase and amphibole, and smaller Fe-Ti oxides set into a rhyolitic interstitial glass. (c) Deformed rock specimen from the fault zone (marked with a cross on main photo), showing intense shearing of plagioclase phenocrysts and breakdown of amphibole.

$0.1–4 \times 10^5\ m^3\ d^{-1}$, equivalent to ascent rates of $0.008–0.13\ m\ s^{-1}$ [*Venezky and Rutherford*, 1999; *Noguchi et al.*, 2008; *Cichy et al.*, 2010]. The eruption was punctuated by two distinct phases of spine growth, at the onset of the eruption (20–21 May 1991) when extrusion rate was at its highest and at the end of the eruption (mid-October 1994 and mid-February 1995) when spine growth was measured at an average of $0.8\ m\ d^{-1}$ [*Yamashina et al.*, 1999]. The late spine extrusion was accompanied by 40–60 h inflation/deflation cycles and vigorous seismic swarms at depths generally shallower than 0.5 km [*Yamashina et al.*, 1999; *Umakoshi et al.*, 2008], constrained to originate from pressure fluctuations at 0.7–1.3 km depth [*Hendrasto et al.*, 1997; *Kohno et al.*, 2008]. The final spine grew to a total of 150 m wide, 30 m deep, and 40 m high [*Nakada et al.*, 1999], preserving a record of the deformation mechanisms acting during magma ascent. A structural survey of the relict spine [*Smith et al.*, 2001] exposed a range of ductile and brittle deformation structures, including shear zones with complex dilational structures (contributing to the permeable network), sintered breccia, and shear zones hosting cataclasite (Figure 2a). Close examination of the fault zone compared to the undeformed lava core (Figure 2b), reveals a heavily damaged rock, with sheared plagioclase crystals and few visible amphibole fragments (Figure 2c).

The dome and spine material is dacitic (65 ± 1.5 wt.% SiO_2) and contains 24–35 vol.% phenocrysts, dominantly plagioclase, amphibole, and biotite together with iron-titanium oxides and quartz in a groundmass containing 40 ± 10 vol.% microlites within a peraluminous rhyolitic interstitial glass containing ca. 78 wt.% SiO_2 [*Nakada and Motomura*, 1999; *Almberg et al.*, 2008; *Cordonnier et al.*, 2009]. The glass transition (estimated on the

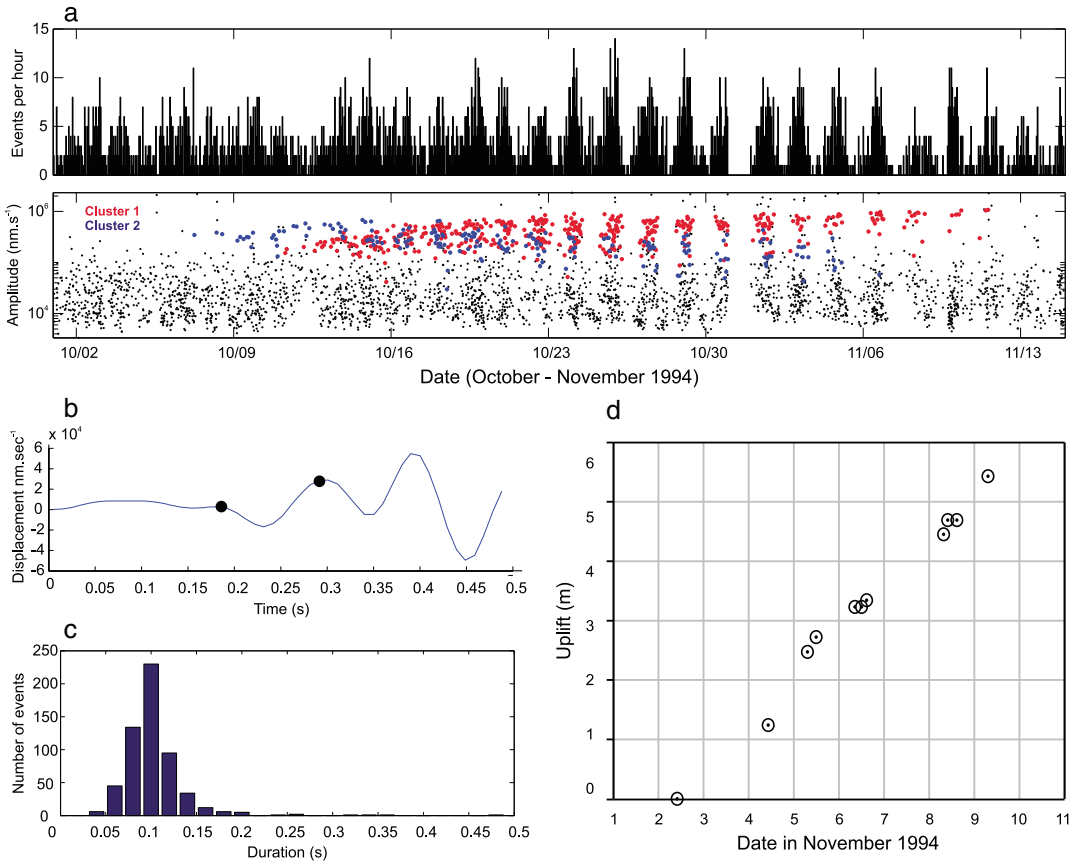

Figure 3. Geophysical data showing (a) hourly counts (above) and amplitude (below) for all seismic events from 1 October to 15 November 1994. A periodicity in event count peaks emerges on 15 October. We highlight the clustering of two waveform families (multiplets of five or more events with very similar waveforms) marked in red (cluster 1) and blue dots (cluster 2). (b) *P* wave pulse duration taken from the first arrival at the point of maximum curvature to the peak where the acceleration gradient falls again to zero. (c) Histogram of *P* wave pulse durations for all events in families 1 and 2 (binned with 0.02 s intervals). (d) Uplift of the spine between 11:00 A.M. on 2 and 11:00 A.M. on 9 November 1994 from time-differential stereoscopic measurements, adapted from *Yamashina et al.* [1999].

basis of a viscosity of 10^{12} Pa s) is constrained to 759°C using the chemical composition within the viscosity model of *Giordano et al.* [2008]. Note that the glass transition is higher when considering heating rates and strain rates as high as those presented in this study and would approximate values some 200–250°C higher at heating rates of ca. 300–400°C s^{-1} [cf. *Gottsmann and Dingwell*, 2001].

2. Methods

2.1. Seismic Analysis of Fault Friction at Mt. Unzen

We analyzed the continuous seismic records from one station (FG1) for the period 1 October 1994 to 28 February 1995 using the GISMO MATLAB suite [*Reyes and West*, 2011] and performed single-station detection (SSD) on the data using a short-term average/long-term average (STA/LTA) algorithm (Figure 3). Seismic station FG1 was chosen as the best candidate for use as a master station in SSD due to its consistent operation and its proximity (~0.6 km) to the lava dome [*Umakoshi et al.*, 2008]. Event rates, peak amplitude, and frequency index (FI) metrics were used to characterize identified seismic events. Event rates were computed on an hourly basis by counting the events that fall within hour-long bins. Peak amplitude was determined from the highest absolute value of demeaned event waveform data. FI is a spectral ratio defined as follows:

$$\mathrm{FI} = \log_{10}\left[\frac{\mathrm{mean}(A_{\mathrm{upper}})}{\mathrm{mean}(A_{\mathrm{lower}})}\right] \quad (2)$$

which was designed to provide a consistent classification of seismic events [*Buurman and West*, 2010]. This method uses the ratio of the mean spectral amplitude in two predefined spectral bands, A_{upper} and A_{lower}, to describe the relative partitioning of energy at high and low frequencies for a given event. To identify earthquake clusters (families of events with similar waveforms, also known as multiplets) from the series of SSD events, we used a cross-correlation technique with a hierarchical clustering scheme. This scheme was successfully employed to detect clusters at Augustine [*Buurman and West*, 2010] and Redoubt [*Ketner and Power*, 2013] volcanoes. To be successfully included in a cluster, an event must have a minimum mean correlation value of 0.8 with all the other events in the cluster. A threshold of five events was used to define the minimum number needed to compose a cluster. Source durations were estimated from manual picking of the *P* wave pulse duration for each event (Figure 3c). Estimates of average fault slip velocity were obtained from measurements of average source duration and slip distance per event. In order to estimate the average slip distance associated with a single seismic event, we considered the total event count for clusters over two periods in early November 1994 (assuming that all these events originated from faulting along spine walls during extrusion; see discussion in section 4.2) during which vertical spine extrusion was recorded using time-differential spectroscopy and theodolite surveys [*Japanese Meteorological Association*, 1995; *Yamashina et al.*, 1999].

2.2. Fault Friction Experiments

The frictional properties of Mt. Unzen dacite were investigated using two low- to high-velocity rotary shear (HVR) apparatuses. The sample block was collected from a block-and-ash flow deposit during a field campaign in 2008 and has mineralogy akin to that described in *Nakada and Motomura* [1999] and *Almberg et al.* [2008], with $<$40 vol.% glass, a density of 2505 kg m^{-3}, and ~13 vol.% porosity as measured by a Micromeritics He-Pycnometer. The HVR setups use a concentric sample geometry and are capable of rotation rates from ~1 rotation per year up to 1500 rotations per minute (rpm) and applied normal force up to 10 kN [*Shimamoto and Lin*, 1994; *Tsutsumi and Shimamoto*, 1997]. In this study, high slip rate ($>$0.4 m s^{-1}) tests were performed with the first-generation HVR at the Kochi/JAMSTEC Core Center (Japan) and low slip rate ($<$0.4 m s^{-1}) tests were performed with the second-generation HVR at the University of Liverpool (UK). We prepared hollow cylindrical samples with 25 mm outer diameter and 10 mm inner diameter to create an ~7.5 mm wide annular contact surface; this minimizes the effect of variable shear resistance produced by a gradient in strain rate (see Figure 4a). Displacement rate was calculated using an equivalent rotational rate, V_e (m s^{-1}), defined such that $\tau V_e S$ gives the rate of total frictional work (where τ is shear stress and S is the fault area), assuming constant shear stress across the fault surface [after *Shimamoto and Tsutsumi*, 1994]:

$$V_e = \frac{4\pi R\left(D_o^2 + D_i D_o + D_i^2\right)}{3D_o + D_i} \tag{3}$$

where R is the revolution rate (s^{-1}), and D_o and D_i are the samples' outer and inner diameters, respectively. We conducted the HVR experiments at six slip rates (0.001, 0.01, 0.1, 0.4, 1.0, and 1.45 m s^{-1}) and five normal stresses (0.4, 1.0, 2.0, 3.0, and 3.5 MPa) for a total of 20 m of slip. During the experiments, the shear stress, normal stress, and shortening were recorded at 500 Hz. Prior to high slip rate tests, the sliding surfaces were ground parallel over ~200 revolutions at 0.1 MPa and 0.1 m s^{-1}, and each sample was bound with aluminum wire to reduce the tendency for fracturing by thermal expansion during experiments at high load. Axial stresses $>$3.5 MPa led to failure at the onset of rotation as high torque, thermal fracturing [*Ohtomo and Shimamoto*, 1994], and high initial fracture density of the samples [e.g., *Cordonnier et al.*, 2009] caused the sample strength to be overwhelmed. The experiments were recorded with optical and infrared thermographic cameras throughout the experiment. For experiments in Kochi/JAMSTEC Core Center, we employed a H2406 NEC\Avio thermographic infrared camera with 90 μm pixel size at 30 frames per second and analyzed the images using InfReC Thermography Studio. For the experiments in Liverpool, we used a FLIR X6000sc thermographic infrared camera and analyzed the images using the FLIR IR Max software package. For all thermal videos, the maximum pixel temperature was tracked through time, as a lower bound for temperature along the slip zone. It is important to note that the monitored surface temperatures slightly underestimate the actual temperatures generated along the slip interface inside the samples (see section 3.5).

2.3. Frictional Melt Structure, Chemistry, and Rheology

The frictional melt layers that solidified into glassy pseudotachylytes were examined using optical microscopy on thin sections cut tangentially to the sample annulus. The fraction, size, and aspect ratio of

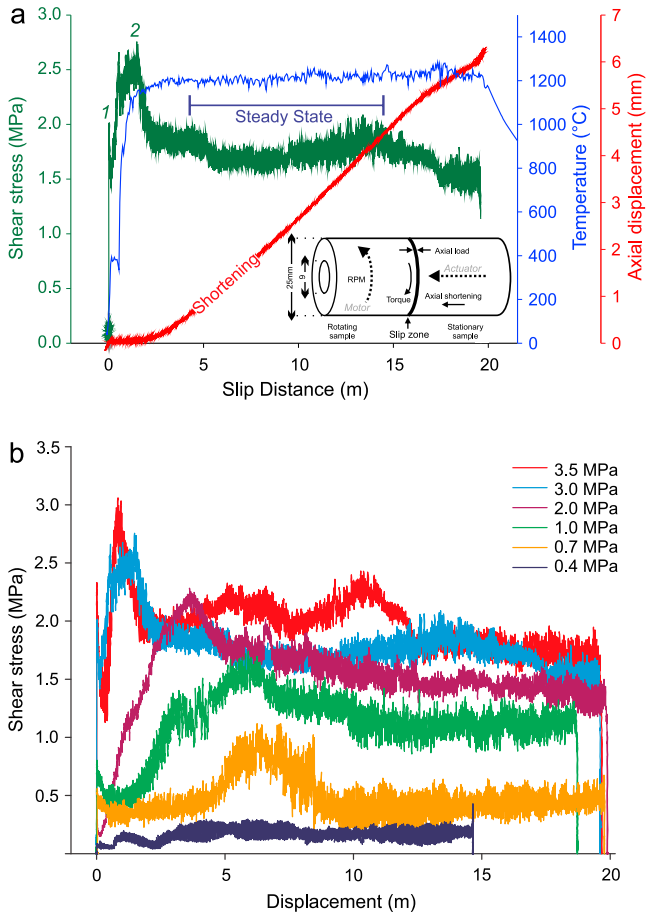

Figure 4. (a) Characteristic mechanical data monitored during a high-velocity rotary-shear experiment undergoing frictional melting, from experiment 3376 (conducted at 1.45 m s^{-1} and 3.0 MPa). The first and second peaks referred to in the results are labeled 1 and 2. Note stabilization of temperature, shear stress, and shortening rate during steady state slip. The inset details the sample setup, showing the directions of applied forces and measurements [modified from *Hirose and Shimamoto*, 2005]. (b) The mechanical data for all experiments conducted at 1.45 m s^{-1} slip rate reveal a systematic increase in shear resistance with applied normal stress. For the data at an applied stress of 0.4 MPa, no second peak in shear stress was observed and the applied slip dynamics did not induce frictional melting.

the comminuted crystalline phases were measured by converting cross-polarized photomicrographs (using a Leica 2500P microscope under transmitted light at 10X zoom) of the center of each slip zone into binary images using the open source software ImageJ. We assigned cumulative crystal fragment area by aspect ratio bins to determine the crystal size distribution within the pseudotachylytes. The thickness of melt layers is required to calculate strain rates, but thickness cannot be estimated directly during a test, and we revert to measuring the average thickness of the solidified glass layers as a proxy, although this represents a minimum value as a certain amount of melt may have been extruded upon cooling at the end of the test [e.g., *Hirose and Shimamoto*, 2005].

Chemical analysis and imaging were performed using a Cameca SX100 electron microprobe. Measurements were made on polished thin sections prepared from eight postexperimental samples. For the homogenized slip zones, we conducted measurements using a 10 μm defocused beam with 15 kV accelerating voltage and 5 nA sample current. For each thin section, ~30 points were chosen on the glass of the experimentally generated pseudotachylyte: near the center of each thin section and away from crystals. However, for sample 3758 (with low melt generation), 12 additional measurements were performed under shortened acquisition time with a focused beam. In order to assess and thereby minimize the potential loss of alkalis, we compared analyses made with focused and defocused beams. The water content present in the glass was estimated through measurement of thermogravimetric weight loss using a simultaneous thermo-analyzer (Netzsch STA Jupiter 449 F1 with a resolution of 25 ng). The change in mass of a 0.19 g sample of glass produced from experiment HVR 3376 (1.45 m s^{-1} at 3 MPa) was measured during heating in an argon atmosphere to 1150°C at 10°C min^{-1} with a dwell time of 180 min.

The temperature dependence of viscosity of the frictional melt was calculated using mean major element compositions and volatile content of the pseudotachylyte glass as inputs into the melt viscosity model developed by *Giordano et al.* [2008]. The apparent viscosity of the frictional melt suspension was estimated using the strain rate-dependent rheological model for magma suspensions of *Costa et al.* [2009] with fitting parameters solved from the experimental data of *Caricchi et al.* [2007]. Maximum packing fraction of the clast population was estimated using the aspect ratio distribution within the model of *Mueller et al.* [2011]. Minimum and maximum values of strain rate (as described by the slip rate and minimum and maximum solidified melt thickness across the sample contact area) and crystal content were considered.

We estimated the mechanical importance of frictional melt viscosity by comparing modeled values of apparent viscosity to viscosity experimentally determined via the steady state shear stress to strain rate ratio [see also *Violay et al.*, 2014].

3. Results

3.1. Seismicity During Spine Growth

Spine extrusion at Mt. Unzen was accompanied by vigorous seismic activity (Figure 3a). Clear cyclic patterns in seismicity can be seen in the early part of the record (13 October to 15 November 1994) where peaks in event count are separated by approximately 48 h periods. Cross correlation of all the events in this period found 29 clusters of 5 to 481 events (see Figures 3a and 3b). The two largest clusters (cluster 1, containing 481 events and cluster 2, containing 187 events) contain 73% of all clustered events from 1 October to 15 November (Figure 3b) and coincided with the emergence of the spine and onset of cyclicity in earthquake occurrence rates. Cluster 2 began several days before visible extrusion of the spine in mid-October and was characterized by repetitive bursts of seismic activity until 5 November. Cluster 1 contains the majority of seismic events throughout this period, showing near-continuous activity until 20 October, before evolving into a repetitive pattern of periodic bursts in concert with cluster 2 (Figure 3b). Events in cluster 1 show steadily increasing amplitudes up to mid-November, distinct from nonclustered events (Figure 3b). These results point to a nondestructive and repetitive source mechanism for the clustered seismic events in the early period of spine growth. The distinct increase in amplitude suggests an increasing fault plane area or a shallowing source during spine extrusion. Seismic activity decreased after mid-November and was associated with a drop in extrusion rate until activity ceased in February 1995. During the period from 11:00 A.M. on 2 November to 11:00 A.M. on 9 November, 61 seismic events from clusters 1 and 2 occurred concurrently with observed uplift of 5.43 m, indicating an average slip distance of 8.9 cm per event (Figure 3e). The *P* wave pulse durations of earthquakes in clusters 1 and 2, shown in Figure 3d, average at 0.118 s and show a strong bunching around this value; hence, this average value is suitably robust for our calculations (Figure 3c). These measurements indicate that average slip rate of the clustered events was 0.75 m s^{-1}, a rate similar to that constrained for other spine extrusions [*Kendrick et al.*, 2012, 2014a].

3.2. High-Velocity Rotary Shear Experiments

Shear experiments performed to assess the frictional properties of Mt. Unzen dome material have shown that at low slip rates ($<$0.4 m s^{-1}) and normal applied stress ($<$0.4 MPa), rock-rock friction takes place and cataclastic gouge forms within the slip zone, and that at higher slip rates and normal applied stresses, melting ensues along the slip interface (Table 1). Rock-rock friction is characterized by an initial peak in shear stress, followed by a rapid decrease (see data for $\leq$0.4 MPa normal stress in Figure 4a and supporting information Figure S1). Beyond this brief weakening stage, the shear stress stabilizes. During experiments which triggered frictional melting, the shear resistance further evolves, showing a progressive increase in shear stress as melt pockets spread along the slip zone. Visible growth of a melt layer across the entire slip zone corresponds with a second, higher, peak in shear resistance. The melt layer subsequently thickens, and melt begins to be expelled due to centrifugal force and axial load, causing axial shortening (Figure 4a). In the process, the shear stress decreases to a steady state as equilibrium is reached between melt production and expulsion [e.g., *Hirose and Shimamoto*, 2005]. Thermal monitoring during the friction experiments showed that heating of the slip zone increases rapidly, reaching rates of up to 1000°C s^{-1} and achieving melt temperatures of 1180–1290°C during mechanical steady state (Figure 4a). Normal stress and slip distance exhibit important controls on the shear resistance imposed by the rock or melt (Figure 4b).

The cumulative data set for all experiments is plotted in shear stress to normal stress space for the monitored peak (Figure 5a) and steady state (Figure 5b) shear stresses. Byerlee's frictional law [equation (1)] is accompanied by modeled curves of the dependence of both slip rate (V_e) and normal stress (σ_n) on the shear resistance (τ) using the relationship $\tau = 0.8e^{-0.42V_e}\cdot\sigma_n$ (where 0.42 is a coefficient with units s m^{-1}) empirically constrained for Mt. Unzen ash gouge [*Lavallée et al.*, 2014]. Both peak shear resistance and steady state shear resistance increase systematically with normal stress as predicted by Byerlee's friction law, although a considerable deviation from a linear relationship in peak shear stress is induced by high slip rates and, importantly, the generation of frictional melt along the slip surface. We note that the peak in shear stress can be extremely high (inducing a state where $\sigma_n/\tau > 1$) when a melt layer first forms. Peak shear resistance remains

Journal of Geophysical Research: Solid Earth

10.1002/2014JB011660

Table 1. Summary of Experimental Conditions Together With Mechanical, Thermal, and Axial Shortening Data Measured During the Experimental Runs

Experiment No.	Equivalent Slip Rate V_e (m s^{-1})	Normal Stress σ_n (MPa)	Max Shear Stress σ_p (MPa)	Steady State[a] Shear σ_{ss} (MPa)	Max Recorded Temperature (°C)	Total Slip Distance (m)	Melt Zone Width w (μm)[b]	Strain Rate $\dot{\varepsilon}$ (s^{-1})	Clast Fraction ϕ	Clast Aspect Ratio[c] R_p	Melt Viscosity[d] η_m (log Pa s)	Mean Power Density Ω_p (MW m^{-2})	Viscosity Measured by HVR[e] η_{HVR} (log Pa s)
3375	1.450	0.4	0.212	0.175	259.0	14.7	–	–	–	–	–	0.236	–
3758	1.450	0.7	0.950	0.413	969.4	19.8	100	1.5E+04	0.20	1.6; 2	2.82	0.804	1.82
3373	1.450	1.0	1.573	1.115	1281.6	18.7	100	1.5E+04	0.08	–	2.95	1.249	2.04
3755	1.450	2.0	2.192	1.524	1285.6	19.9	100	1.5E+04	–	–	2.88	1.611	2.18
3376	1.450	3.0	2.549	1.732	1284.2	19.6	150	9.7E+03	0.12	–	2.85	3.039	2.42
3384	1.450	3.5	2.806	1.944	1286.7	19.7	100	1.5E+04	0.09	–	2.96	2.941	2.29
3378	1.000	0.4	0.303	0.243	532.3	16.4	–	–	–	–	–	0.245	–
3757	1.000	0.7	0.893	0.432	1117.8	21.3	–	–	–	–	–	0.354	–
3365	1.000	1.0	1.550	0.851	1156.6	18.6	–	–	–	–	–	0.778	–
3359	1.000	2.0	2.342	1.339	1264.3	19.0	150	6.7E+03	0.16	1.5; 2.2	2.75	1.160	2.55
3370	1.000	3.0	2.253	1.847	1267.0	19.0	100	1.0E+04	0.08	–	2.81	2.086	2.35
3382	1.000	3.5	2.512	2.209	1268.6	19.2	150	6.7E+03	0.22	1.4; 1.8	2.95	1.630	2.58
3379	0.400	0.4	0.183	0.155	193.6	19.1	–	–	–	–	–	0.064	–
3369	0.400	1.0	0.669	0.584	650.8	19.1	–	–	–	–	–	0.221	–
3363	0.400	2.0	1.195	0.965	1128.1	19.1	–	–	–	–	–	0.366	–
3372	0.400	3.0	1.794	1.574	1187.3	19.0	150	2.7E+03	0.18	1.4; 2	–	0.593	2.83
0046	0.001	0.4	0.400	0.205	–	1.4	–	–	–	–	–	–	–
0047	0.010	0.4	0.300	0.238	–	7.1	–	–	–	–	–	–	–
0048	0.100	0.4	0.305	0.169	–	21.5	–	–	–	–	–	–	–
0049	0.001	0.7	0.461	0.407	–	1.4	–	–	–	–	–	–	–
0051	0.010	0.7	0.625	0.599	–	7.1	–	–	–	–	–	–	–
0052	0.100	0.7	0.586	0.315	–	14.2	–	–	–	–	–	–	–
0053	0.001	1.0	0.780	0.739	–	1.4	–	–	–	–	–	–	–
0056	0.010	1.0	0.854	0.686	–	7.1	–	–	–	–	–	–	–
0054	0.100	1.0	0.490	0.396	–	6.2	–	–	–	–	–	–	–

[a]The values of shear stress at steady state refer to equilibrated values after complete melting.
[b]Average solidified melt zone width estimated from photomicrographs—a lower bound for melt zone width during steady state slip (see section 2).
[c]Bin size 0.2 determined by mean normalized to area fraction; for bimodal aspect ratio distributions, both values are given.
[d]Melt viscosity values are quoted for a single temperature (1300°C) using the model of *Giordano et al.* [2008].
[e]Viscosity calculated as shear stress/strain rate mechanically measured in the HVR tests for steady state conditions.

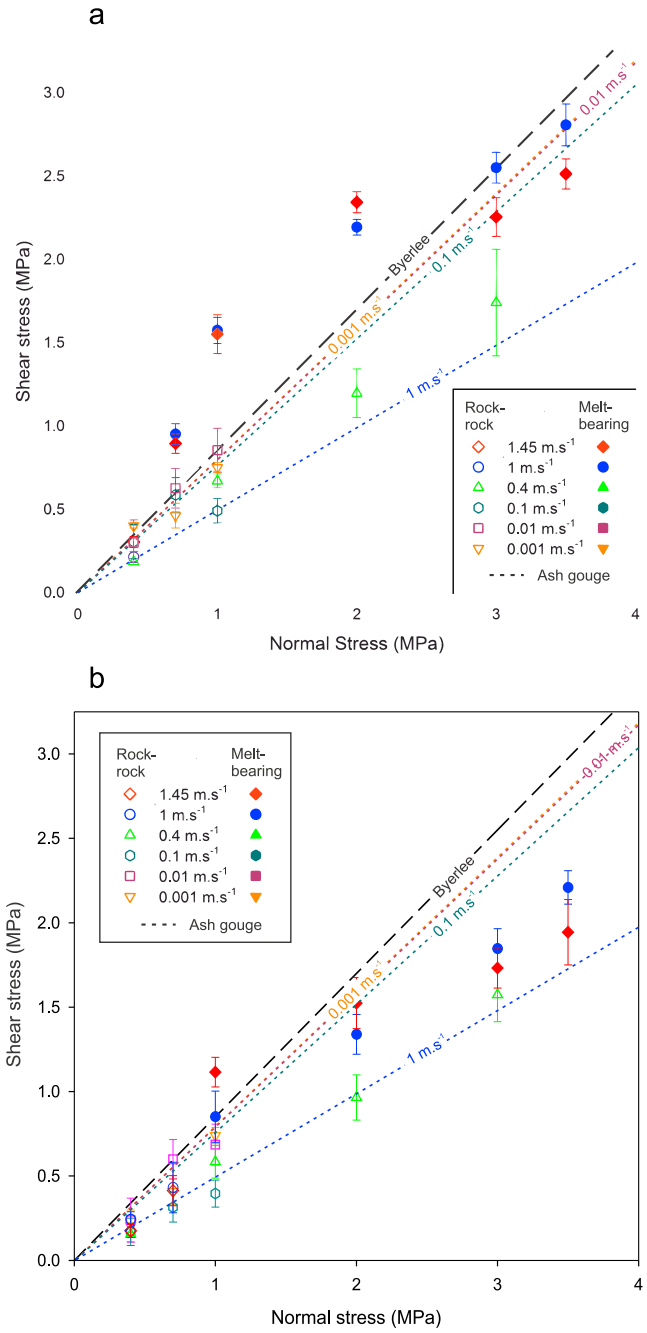

Figure 5. Shear resistance in rock-on-rock and melt-bearing faults. The data set highlights (a) the peaks and (b) the steady state shear stress monitored during slip for all experiments. The data are plotted together with Byerlee's law for rock friction (black dashes) as well as the empirically modeled frictional response of Mt. Unzen ash gouge as a function of slip rate shown as colored dotted lines [*Lavallée et al.*, 2014].

particularly high during the steady state slip at low normal stresses (<3 MPa), where melt plausibly acts as a brake [e.g., *Kendrick et al.*, 2014a]; for higher normal stress, the shear stress tends to fall to values below those predicted by Byerlee's law, implying that frictional melt acts as a lubricant to slip compared to the internal friction of intact rocks [*Di Toro et al.*, 2006a]. Lubrication within the steady state reduces the normal stress dependence on friction compared to Byerlee but not to the extent demonstrated in previous studies on crustal rocks [*Di Toro et al.*, 2006b; *Nielsen et al.*, 2008]. It is also remarkable that an increase in slip rate (for a given applied normal stress) does not necessarily lead to a decrease in shear stress as would be expected from the non-Newtonian, shear thinning rheology of the multiphase melts produced by friction [*Lavallée et al.*, 2012].

The combined effect of slip rate [equation (2)] and applied normal stress on the resultant friction coefficient is assessed by analyzing the mean power density (Ω_p) produced in the experiments, as follows:

$$\Omega_p = V_e \tau_p \quad (4)$$

where τ_p is the average shear stress [*Di Toro et al.*, 2011]. For the purpose of this analysis, where melting occurred, the mean power density was calculated from the average shear stress from the onset of slip to peak shear stress due to melting, whereas for experiments without melting, the average shear stress of the full data was used. The slip distance required to generate a complete melt layer along the slip zone decreased as normal stress and/or slip rate increased (Figures 4b and 6). As such, the mean power density becomes a more informative measure of the conditions prompting melting. At the lowest mean power densities (<0.3 MW m^{-2}), frictional melting did not occur. Experiments with mean power density of 0.3 to 1 MW m^{-2} reached temperatures sufficiently high to induce melting over slip of a few meters (Figure 6). Experiments with higher power density ≥1 MW m^{-2} reached higher maximum temperatures of ~1285°C with near instantaneous melt production (Figure 6). We note that the maximum temperature during steady state slip on melt-hosting slip zones remained constant, independent of imposed conditions—an observation which facilitates a rheological description of fault slip dynamics.

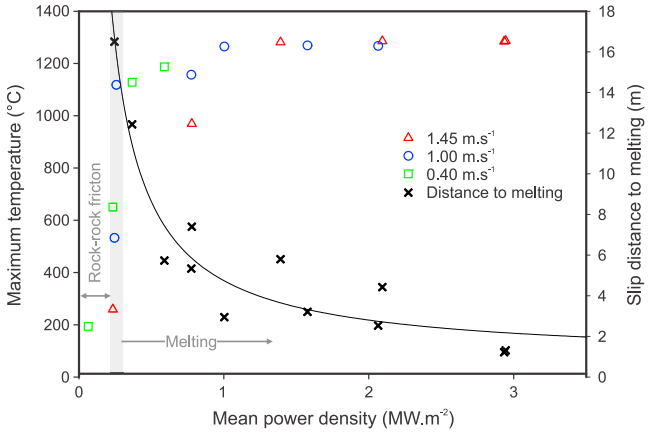

Figure 6. Thermal budget and melting propensity during HVR friction experiments. The data shows that at $\Omega_p > 0.3$ MW m^{-2}, the maximum monitored temperature reaches a plateau, which coincides with observations of frictional melting on the fault plane. Experiments with $\Omega_p < 0.3$ MW m^{-2} did not achieve temperatures sufficient for melting on the slip plane. The total slip required to achieve frictional melting decreases nonlinearly with increasing mean power density (solid line shows best fit to the data).

3.3. Microstructural Analysis of Experimental Products

Thin sections from experimental samples that developed a frictional melt layer were prepared for optical and geochemical analyses. The frictional melt layers (solidified into glasses) exhibit a distinct change in texture from the surrounding protolith; the pseudotachylyte glass hosts crystal fragments (primarily of plagioclase) with a lower aspect ratio and smaller size than in the host rock. Importantly, amphiboles are not present in these layers. The thickness of the solidified melt zones ranges from 75 to 300 μm, but does not vary systematically with experimental conditions, and can differ by >100 μm across a given sample. The characteristics of the rock-melt boundary as well as of the pseudotachylyte layer itself reveal a dependence on the local mineral assemblage. The boundary is generally defined by relatively straight margins, though a few irregular embayments likely result from existing heterogeneities in the host rock. This is particularly enhanced by the presence of large amphibole phenocrysts (up to 5 mm diameter), which preferentially decompose along the melt-rock interface (Figure 7a). The boundary observed in our experimental products is not as sharp as those observed in holocrystalline rocks [*Hirose and Shimamoto*, 2003, 2005], and we note the progressive alignment of microlites near the slip plane, associated with viscous remobilization (Figure 7b) as local temperatures are sufficient to exceed the glass transition of the neighboring groundmass glass without inducing melting (see section 4.1). Crystal fragments in the experimental pseudotachylytes are generally angular, suggesting the occurrence of cataclasis and short periods of interaction with the melt [*Bizzarri*, 2014]. The crystal fragments are dominated by plagioclase, while ferromagnesian oxide minerals are scarcer than in the host rock and amphibole is not seen: observations that indicate preferential melting of amphibole and ferromagnesian minerals. Particle size distribution was estimated on between 480 and 3314 suspended crystal fragments for each experimentally produced pseudotachylyte layer. The layers contain between 8 and 22 vol.% particles with local variation reaching >5 vol.% (see Table 1). Cumulative particle size (binned by aspect ratio) shows that the particle shape distribution is weakly bimodal, with aspect ratio peaks at approximately 1.6 and 2.0 (see supporting information Figure S2).

Scanning electron microscope (SEM) analysis reveals chemical and physical homogenization of the frictional melt solidified at the end of the experiments. All but one experimental pseudotachylyte (experiment 3758, at 1.45 m s^{-1} and 0.7 MPa, which did not reach a steady state after melting) show a near-homogeneous suspension with minor chemical heterogeneities, seen in the grey-scale exhibited by the interstitial glass, and the presence of small pores near the rock-melt boundaries (Figure 7c). The pseudotachylyte from sample 3758 shows a range of suspended clast sizes, iron content, and thickness (Figure 7d): a thin layer of protomelt (i.e., an inhomogeneous melt band resulting from single crystal melting) containing smaller crystal fragments is surrounded by a thicker, homogeneous, solidified melt zone. The groundmass of the host rock in this experiment does not show evidence for viscous remobilization (Figure 7d), as seen in other samples, suggesting that the host rock in this particular example did not surpass the glass transition temperature and strain was localized in the protomelt along the inner slip interface only.

3.4. Geochemistry of Frictional Melt

Electron microprobe analysis reveals that these experimentally produced frictional melts have similar compositions, with the exception of the aforementioned heterogeneous pseudotachylyte produced in

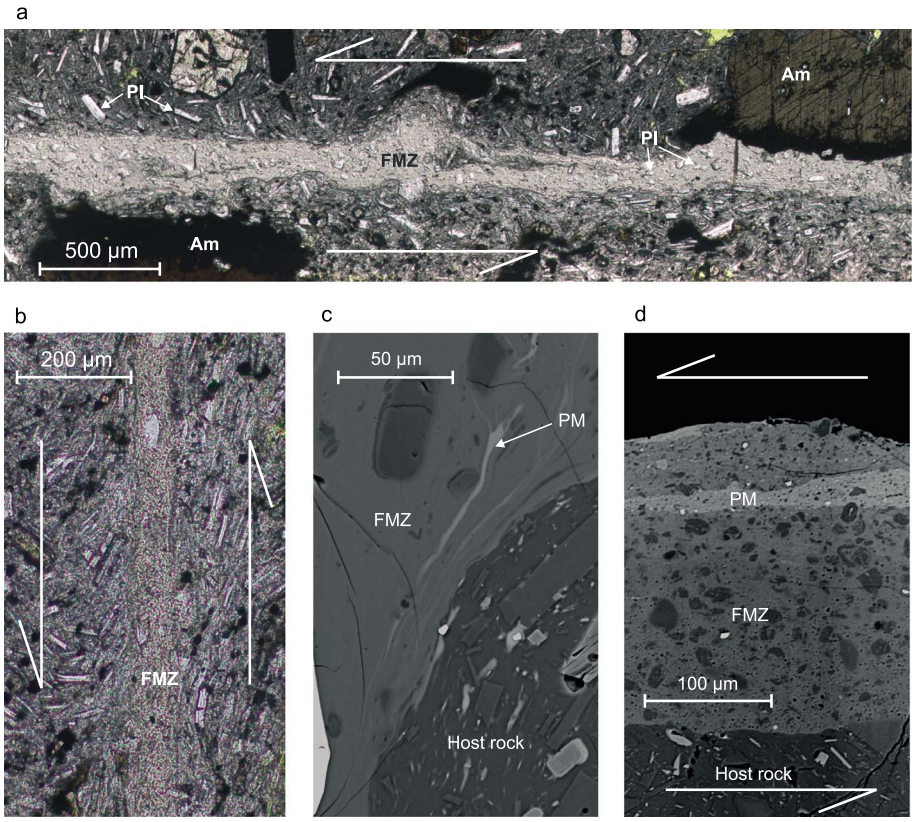

Figure 7. Microtextural characteristics of frictional melt zones. (a) Photomicrograph of a typical frictional melt zone (FMZ) from experiment 3376 (conducted at 1.45 m s^{-1} and 3 MPa), showing suspended angular plagioclase fragments (Pl) and adjacent amphibole phenocrysts (Am). The edge of the melt zone exhibits an embayment (in the upper middle) and a dark rim along the amphibole, suggestive of thermal breakdown. (b) Close-up image from experiment 3373 (1.45 m s^{-1} and 1 MPa normal stress), showing crystal rotation in the host rock along the outer margin of the frictional melt layer due to viscous remobilization in areas where temperatures exceeded the glass transition. Arrows indicate the direction of slip. (c) SEM image showing an inhomogenized melt filament due to selective amphibole melting (light grey) inside the main frictional melt zone (darker grey) from experiment 3359 conducted at 1.0 m s^{-1} and 2.0 MPa. (d) SEM image of melt zone in sample 3758 (1.45 m s^{-1} and 0.7 MPa), showing a protomelt within a crystal-rich frictional melt zone.

sample 3758 (Table 1). This single heterogeneous product has substantially lower SiO_2 and Al_2O_3, and higher MgO and FeO contents: differences suggesting selective melting of amphiboles and ferromagnesian minerals (Table 2). The volatile content of the pseudotachylyte glass is low (0.1 wt.%) as ascertained by simultaneous thermo-analysis, which shows no detectable weight loss up to 1150°C (0.1% relative mass increase is likely due to iron oxidation) concordant with water analysis of the bulk rock of ~0.1–0.2 wt.% [*Kusakabe et al.*, 1999; *Nakada and Motomura*, 1999; *Noguchi et al.*, 2008].

3.5. Rheological Analysis of Frictional Melt

An accurate description of the rheological impact of frictional melt on fault slip behavior requires a detailed description of the viscosity of the melt. The temperature-dependent viscosity range of the frictional melts, calculated based on their chemical composition and using a melt viscosity model [*Giordano et al.*, 2008], shows little variation (Figure 8). Viscosities derived from this model fall between 10^3 and $10^{3.5}$ Pa s; however, these are likely slightly overestimated, because of underestimated temperatures due to cooling of melt at the sample exterior. Notably, the calculated viscosity of the inhomogenized melt from experiment 3758 (see Figure 7c) is significantly lower than the other "homogenized" frictional melts. The rate-dependent apparent viscosities of the frictional melt suspension were constrained for the sample-specific crystal fraction and strain rate estimates in the solidified melt zones (Table 1), using the semi-empirical model of, and fitting parameters within, *Costa et al.* [2009]. A maximum packing fraction of 0.55 was estimated from the model of *Mueller et al.* [2011] using an aspect ratio of 1.8 (supporting

Table 2. Electron Microprobe Measurements Showing Major Oxide Compositions From Experimental Frictional Melts[a]

	Interstitial Glass Composition of Experimental Pseudotachylyte										Starting Material	
	3359	3370	3373	3376	3382	3384	3755	3758	3758ii Main[b]	3758 Protomelt[b]	2007B Bulk Rock	Interstitial Glass[c]
SiO_2	64.98	64.21	65.86	64.70	65.80	64.77	65.47	64.58	62.41	51.20	63.87	78.34
TiO_2	–	–	–	–	–	–	–	–	–	–	0.66	0.43
Al_2O_3	15.02	16.30	14.86	15.20	14.77	17.11	14.94	16.38	15.41	10.95	16.54	11.88
FeO(T)	5.44	4.64	5.03	5.01	4.92	4.16	5.22	4.90	6.48	12.40	5.07	0.84
MnO	–	–	–	–	–	–	–	–	–	–	0.11	0.03
MgO	3.78	3.30	3.34	3.37	3.27	2.57	3.36	3.14	4.41	10.66	2.72	0.09
CaO	5.48	5.44	4.66	5.31	5.08	5.53	5.07	5.78	6.39	9.67	5.39	0.49
Na_2O	3.30	3.60	3.32	3.35	3.33	3.77	3.39	3.45	3.15	1.96	3.55	3.06
K_2O	2.38	2.35	2.70	2.36	2.42	2.19	2.47	2.20	2.10	1.22	2.24	4.79
P_2O_5	0.22	0.15	0.16	0.15	0.17	0.14	0.18	0.19	0.19	0.24	0.17	0.02
H_2O[c]	0.10	0.10	0.10	0.10	0.10	0.10	0.10	0.10	0.10	0.10	0.03	–
F_2O_{-1}	0.00	0.00	0.00	0.00	0.00	0.00	0.00	0.00	0.00	0.00	–	–
Totals	100.59	99.99	99.94	99.45	99.76	100.24	100.10	100.61	100.54	98.30	100.34	99.97
n	20	22	29	29	28	25	22	18	4	4	1	11

[a]The geochemical data are complemented by measurements on interstitial glass in the host rock and X-ray fluorescence (XRF) analysis of the bulk rock chemistry. Results shown are mean values for (*n*) number of measurements. All iron [FeO(T)] is considered as FeO for the microprobe measurements and as Fe_2O_3 for the XRF measurement.
[b]Measurement with focused beam.
[c]Electron microprobe analysis by *Cordonnier et al.* [2009].
[d]Wt.% water estimation based on measurements by *Kusakabe et al.* [1999], *Nakada and Motomura* [1999], and *Noguchi et al.* [2008].

information Figure S2). The low crystal fraction (Table 1) caused only a slight increase in the apparent viscosity of the multiphase frictional melt of $<10^{0.4}$ Pa s.

The mechanical data can be used to estimate the viscosity of frictional melt during torsion experiments [e.g., *Caricchi et al.*, 2007; *Violay et al.*, 2014]. Here by dividing the monitored shear resistance (at steady state) by the calculated strain rate, we obtain a narrow range of apparent viscosity for the frictional melt (η_{HVR}; Figure 8). These values are a lower bound for viscosity, as thickness of the melt may be underestimated due to continued extrusion of melt at the end of the experiment. The obtained viscosity range is compared with the temperature dependence of the modeled viscosity to derive the range of temperatures likely to be found in the slip zone ($T_{HVR} \approx 1320$–1590°C). We find the temperatures constrained from the mechanical data are 50–300°C higher than those monitored using the thermographic camera (T_m) on the surface of the expelled melt (Figure 8); there are discrepancies of ~0.2 to 1 order of magnitude between the values of viscosity estimated from the mechanical data (η_{HVR}) and the values estimated using the monitored temperature (η_m). We note that in this rheological analysis, viscous remobilization of the host rock was not considered; however, the presence of glass-bearing wall rocks has been argued to facilitate viscous coupling to the frictional melt, increasing the shear resistance during faulting events, which could serve to hinder slip [*Lavallée et al.*, 2012; *Kendrick et al.*, 2014a; *Violay et al.*, 2014].

4. Interpretation and Discussion

4.1. Fault Friction: Melting, Viscous Braking, and Remobilization

Here we have constrained spine extrusion at Mt. Unzen to be a fault-driven eruptive process whereby the evolution of the volcanic rocks involved in fault slip is complex. Fault friction of Mt. Unzen dacite falls into the following two regimes: at low mean power densities (i.e., low normal stress and/or slip velocities), slip occurs in the rock-rock regime; above 0.3 MW m^{-2}, the rock-rock slip regime is overprinted by a rheological control on slip when frictional melt forms, accompanied by viscous remobilization of interstitial glass in the adjacent rock. This observation comes with the caveat that power density is an empirical measurement; it determines the thermal energy produced [equation (4) and Figure 6]; however, the temperature of the slip zone depends on the ratio of thermal energy produced to that lost. This depends on the sample properties and geometry, as well as the design and thermal properties of the apparatus. Our key finding, therefore, is a well-constrained threshold in Ω_p over which the slip regime switches from rock-rock to viscous-dominated dynamics. Observations consistent with frictional melting during dome

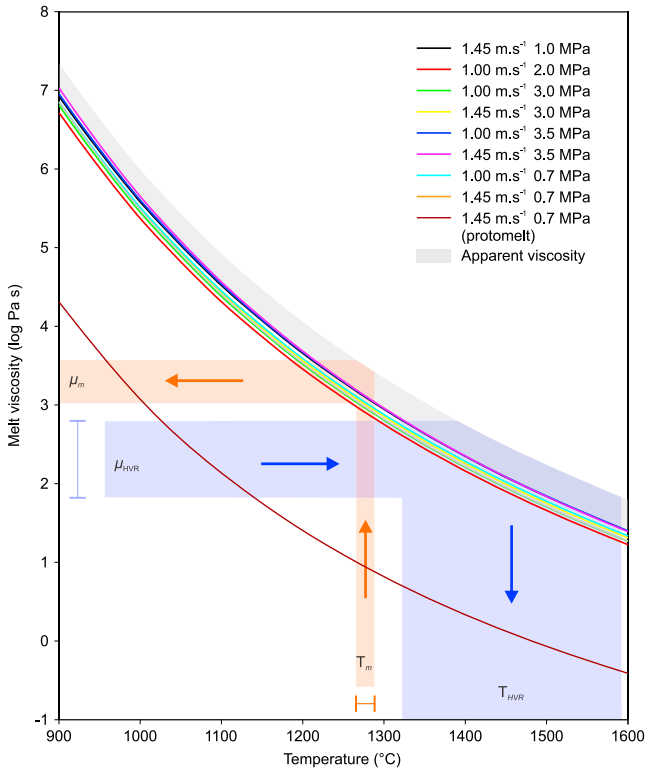

Figure 8. Temperature dependence of melt viscosity calculated from the model of *Giordano et al.* [2008] for nine frictional melt compositions (see Table 1). The apparent viscosities of the frictional melt suspension (grey band) were calculated considering the crystal fraction and strain rate following the method of *Costa et al.* [2009]. We used a maximum packing fraction of 0.55, estimated from the model of *Mueller et al.* [2011], and empirical fitting parameters derived by *Costa et al.* [2009] from the experimental data of *Caricchi et al.* [2007]. This modeled apparent viscosity relationship is compared to the viscosity range mechanically constrained from the steady state regime in the HVR tests (η_{HVR}) which suggests that experimental temperatures (T_{HVR}) reach 1360–1600°C; this temperature is higher than the maximum monitored temperatures (T_m), which on their own would suggest higher operating viscosities (η_m) during fault slip events.

eruptions, and especially spine growth [*Kendrick et al.*, 2012, 2014a, 2014b; *Plail et al.*, 2014], are facilitated by the high temperatures in volcanic conduits [*Lavallée et al.*, 2012]. At Mt. Unzen, groundmass crystallization temperatures have been constrained to 850–870°C [*Venezky and Rutherford*, 1999] and 860–910°C [*Saito and Ishikawa*, 2012] by Fe-Ti oxide re-equilibration temperatures, giving estimated eruptive temperatures ~800°C [*Goto*, 1999]. This suggests that fault slip producing as little as 300°C temperature increase may push slip zone temperatures in excess of 1100°C, and so it appears inevitable that frictional melting and viscous remobilization must be incorporated in dome eruption models.

The friction experiments presented here underline the strong affinity of volcanic rocks for rheological changes due to heat generated through faulting events. Melting occurs due to the very high temperatures achieved along the slip surface, whereas viscous remobilization initiates in the surrounding host at moderate temperatures (above the glass transition temperature, varying between 759°C and 1010°C due to the range of heating rates generated in these experiments), and its extent normal to the slip surface increases as frictional heat dissipates laterally. Such a complex process and associated rheological profile likely play an integral role in strain localization during slip events. The ability of glass to remobilize at moderate temperatures may have important implications during faulting in nature, as a slip event may be able to release enough heat to the surrounding rocks/magma to remobilize larger zones than the localized slip plane. Remobilized areas (Figure 7b) will exhibit high viscosities and non-Newtonian rheology (due to the abundance of microlites and long structural relaxation timescales at moderate temperatures above the glass transition interval), which may induce nonlinearity in shear strain and thus affect the dynamics of magma ascent. Distributed strain partitioning has been observed near the margin of spines (Figure 2) and is commonly attributed to strain experienced by magma in ascent up to the point of failure [*Smith et al.*, 2001; *Pallister et al.*, 2013]; yet the results here are consistent with a scenario in which strain localization also takes place in the slip-dominated region above the locus of shear-induced failure.

Our experiments on dacite affirm previous claims that frictional melting is a highly disequilibrium process [*Spray*, 1993; *Shimamoto and Lin*, 1994]. Early melting initiates in minerals with the lowest melting temperatures at very high heating rates (here 10^2 to 10^3 °C s^{-1}).The generation of protomelts from selective melting of crystals with the lowest melting temperatures suggests that, in the HVR experiments, transient changes in melt composition [e.g., *Spray*, 1993] as well as the evolving contact along the rock-rock to melt-rock surface [e.g., *Hirose and Shimamoto*, 2005] may contribute to changes in shear stress on the slip zone (Figure 4a). Observations of irregular rock-melt boundaries and small crystal fragments in the

solidified melt zones suggest that the preferential melting of amphiboles and subsequent spreading of the melt layer may enhance the suspension of plagioclase fragments in the melt (Figure 7d).

The rheology of frictional melt in the steady state regime appears to be well constrained, as the temperature-dependent melt viscosity is found to be very consistent irrespective of slip conditions (if melting has reached equilibrium with the imposed slip dynamics). The apparent viscosity on the slip zone is also described via the slip rate and clast content; yet the relatively low suspended clast content (8–22 vol.%) induces only a minor apparent viscosity offset of $<$0.5 log units [using the model of *Costa et al.*, 2009]. The viscosities calculated from the mechanical data in this study are 1–2 orders of magnitude lower than the modeled viscosities (see Table 2), an opposite trend to that found in *Violay et al.* [2014], where apparent viscosity measurements were one order of magnitude higher for glassy basalts; however, the absence of water-bearing minerals within this basalt may cause a very different mechanical response. The offset in viscosity measurements in our study may be attributed to one or more of (a) an underestimation on the order of 50–100°C in measured temperature, (b) overestimation of strain rate due to partitioning of strain in viscously remobilized groundmass [e.g., *Violay et al.*, 2014] and due to melt zone thinning from postexperiment melt extrusion upon solidification, and (c) deformation occurring in the brittle regime within the frictional melt.

The analysis presented here portrays a regime in which frictional melting leads to a nonlinear rheological (and hence slip) response, with important implications for spine eruption dynamics. The mechanical control of fault processes in spine growth is likely to be complex as locally fluctuating stress conditions and temperature evolve. In a rock-rock fault regime (low temperature), we observe a linear normal to shear stress relationship for experiments at low slip rates in accordance with Byerlee's frictional law [equation (1)]. Slip is found to be rate weakening, falling further below Byerlee's law with increasing strain rates. In a high-temperature, melt-hosting fault regime, slip rapidly evolves from gouge production to preferential melting of low melting temperature crystals to production of a mature (chemically mixed), steady state melt zone; such changes lead to transient rheology. The mechanical response of frictional melt is highly dependent on the normal stress; while in tectonic settings, frictional melt may offer a lubricating effect (i.e., impart lower resistance than the internal friction of rocks as stated by Byerlee); in shallow volcanic scenarios, low normal stress conditions mean the peak shear stress induced by production of frictional melt can exceed the internal friction of rocks predicted by Byerlee's law and impose a viscous brake [*Fialko*, 2004; *Koizumi et al.*, 2004; *Kendrick et al.*, 2014b].

The contrasting properties of rock-rock and melt-bearing slip zones suggest that fault dynamics in an ascending magmatic column are highly unstable and lead us to conclude that spine extrusion may be hindered when frictional melt forms at the conduit margin. These ascent dynamics may encourage unsteady faulting events (and associated periodic geophysical signals), as a higher shear stress must be generated to overcome the melt-enhanced shear resistance. Thus, the variable frictional properties of volcanic rocks (with or without melting) may have an important role in regulating stick-slip behavior and promote unstable spine extrusion [*Kendrick et al.*, 2014a], providing a feedback to the cyclic deformation patterns seen at Mt. Unzen and other dome-building volcanoes.

4.2. Frictional Controls on Seismogenic Spine Extrusion

The October 1994 to February 1995 extrusion of a spine at Mt. Unzen volcano was monitored by seismic, tilt, and stereoscopic techniques [*Yamashina et al.*, 1999; *Umakoshi et al.*, 2008]. A mechanistic interpretation of these signals requires consideration of the slip mechanics at work in the shallow conduit. Spine extrusion rate from 2 to 9 November 1994 averaged 0.8 m d^{-1} (see Figure 3d), and cycles in the seismic and tilt data, similar to those measured at Soufrière Hills volcano [*Voight*, 1999], suggest pulsatory dynamics where the ascent and extrusion of the spine occurred through incremental slip along an intact plug with minimal strain in its core.

We analyzed the seismic data to provide a constraint on the slip conditions at Mt. Unzen and apply our experimental findings to the monitored eruption dynamics during spine growth. The regular ~48 h cyclicity in seismic event counts (Figures 3a and 3b) indicates a process whereby pressure buildup in the conduit, which leads to inflation, is released by seismogenic fault slip events along the margin of the ascending plug [*Yamashina et al.*, 1999]. Our analysis of the seismic record revealed the importance of two dominant clusters of earthquakes found to take place in periodic cycles. The timing of these cycles shows

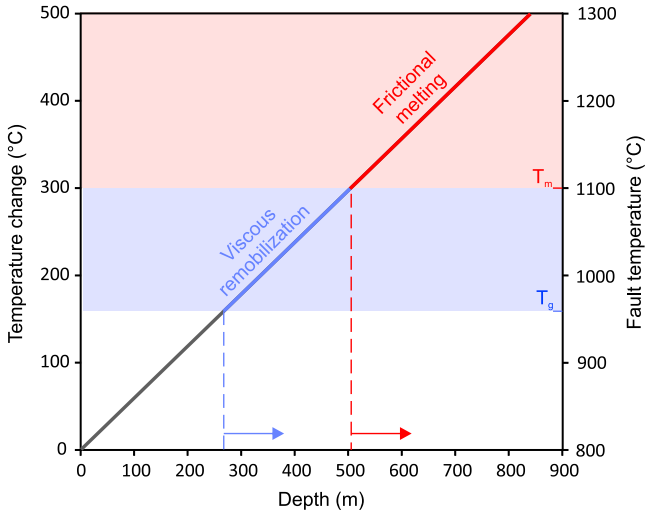

Figure 9. Heat generated by fault friction of an average slip event at Mt. Unzen at varying depth. The left axis shows change in temperature calculated from the equation of *Carlslaw and Jaeger* [1959], from an initial conduit temperature of 800°C. The right axis shows the fault zone temperature. Normal stress on the fault plane is calculated from the lithostatic stress using the equations of *Sheorey* [1994], providing a fault temperature to depth relationship (bold line). Viscous remobilization above T_g is constrained to temperatures exceeding 960°C (blue field), and we highlight a threshold temperature of 1100°C, above which frictional melt forms (pink field). Blue and red dashed lines constrain the minimum depths at which an average fault event during spine extrusion at Mt. Unzen results in viscous remobilization and frictional melt formation, respectively.

a strong correlation with peaks in tilt and total event count, from which we conclude that seismogenic slip events represent the dominant mechanism of uplift during spine growth. The nondestructive source character of the seismicity and similarity of the waveforms suggest a common process occurring within a similar location, from which we surmise that their source mechanism is most likely the brittle failure and slip of magma near the conduit walls at shallow depths [*Yamasato*, 1998; *Varley et al.*, 2010; *De Angelis and Henton*, 2011; *Thomas and Neuberg*, 2012; *Bean et al.*, 2013].

We used our seismic analysis to estimate slip zone properties during spine growth. We find an average slip distance of individual events of 8.9 cm, slip velocity of 0.75 m s^{-1}, and a faulting depth shallower than 700 m below the dome surface [*Japanese Meteorological Association*, 1995; *Umakoshi et al.*, 2008]. From this depth range, we constrain the stress normal to the fault plane using values of the horizontal stress (σ_h), as estimated from the lithostatic stress (σ_l) via *Sheorey* [1994] with E in GPa and z in meters:

$$\frac{\sigma_h}{\sigma_l} = 0.25 + 7E\left(0.001 + z^{-1}\right) \tag{5}$$

where the wall rock elastic modulus (E) is estimated at 10 GPa [*Uhira et al.*, 1995] and z is the depth of interest (0–700 m) providing us with $\sigma_h = 0.42\sigma_l$. Note that the elastic modulus of the magmatic column may differ slightly prior to slip events, but we assume that its elastic response upon faulting at high slip rate would contribute to a value similar to that of a rock [cf. *Lavallée et al.*, 2016]. In our calculation, we use a mean density (ρ) of 2505 kg m^{-3} (measured by He-pycnometry) to constrain stress normal to the fault plane.

In order to solve the problem of heat transfer during slip events (prior to melting), we use the 1-D calculation for temperature change at negligible distance from a heat source (i.e., a slip zone of 0 thickness) derived by *Carlslaw and Jaeger* [1959]:

$$\Delta T = \frac{q\sqrt{t}}{C_p \rho \sqrt{\pi k}} \tag{6}$$

where heat capacity (C_p) is estimated at 1000 J kg^{-1} K^{-1} at 900°C, thermal diffusivity (k) is estimated at 0.7 mm^2 s^{-1} [*Nishimura et al.*, 2005; *Cordonnier et al.*, 2012b], time (t) is constrained by dividing the average slip distance by the slip velocity constrained from the seismicity, and the heat flux (q) is defined as $q = \mu\sigma_n V_e$, in which the coefficient of friction (μ) is set to 0.85 to constrain heat generated from the onset of a slip event at low normal stresses [cf. *Byerlee*, 1978]. The results of these calculations are illustrated in Figure 9, showing the temperature increase plotted against conduit depths for an average slip event. We set a threshold temperature for the onset of frictional melting at 1100°C and an initial conduit temperature of 800°C. This suggests that frictional melting may be viable during fault slip events deeper than 500 m. At shallower depth, we expect that insufficient heat would be produced to melt the rocks by friction; however, enough heat may be generated to viscously remobilize the interstitial glass in these rocks (Figure 9). Considering this

thermal budget of fault slip events, we conclude that it is highly likely that spine extrusion mechanics were modified by viscous forces associated with viscous remobilization and melting during ascent.

4.3. Fault Friction Beyond Melting

Magma ascent is driven by buoyancy, and during spine-building episodes, it is regulated by internal frictional processes. Although the present findings highlight the effect of frictional melting and suggest that it may be a common and important process to be considered, we wish to emphasize that we do not believe that it is the mechanism that controls magma ascent in the entirety of the shallow region for which fault friction influences the eruptive behavior. Field studies have documented the presence of shear zones bordered by fault planes which bear cataclasite, volcanic ash gouge, and breccia near conduit margins [e.g., *Smith et al.*, 2001; *Watts et al.*, 2002; *Kendrick et al.*, 2012; *Kennedy and Russell*, 2012; *Pallister et al.*, 2013]. These result from frictional processes and rapid thermal expansion and stress drops during eruptive activity that lead to fragmentation [e.g., *Alidibirov and Dingwell*, 1996; *Lavallée et al.*, 2011, 2014]. Gouge and polymict breccia found during drilling of the conduit within the intercontinental drilling program are evidence for repeated fragmentation events in the conduit at Mt. Unzen [*Goto et al.*, 2008]. As such, the rheological contribution of frictional melt on slip dynamics must be further combined with the frictional properties of gouge material [e.g., *Moore et al.*, 2008; *Lavallée et al.*, 2014]. The study by *Lavallée et al.* [2014] measured the frictional properties of Mt. Unzen ash gouge, which was found to abide by a simple relationship between normal stress and slip rate (Figure 5a). Energy partitioning into surface creation and granular flow reduces the heat budget in ash-gouge-bearing fault planes, which may inhibit further melting along the slip interface [*Lavallée et al.*, 2014].

The mechanics of slip during spine extrusion at Mt. Unzen are likely variably controlled by frictional melt or gouge within the slip interface at the conduit margin. Our study provides a strong geophysical and thermomechanical argument for the formation of volcanic pseudotachylyte at shallow depths. In addition, we describe the rheology of frictional melt laden fault zones and their potential impact on shallow conduit fault mechanics. Mechanical considerations of fault slip processes have wider implications, as frictional melt generation can occur at lava domes during extrusion [*Kendrick et al.*, 2012, 2014a; *Plail et al.*, 2014], block-and-ash flows [*Grunewald et al.*, 2000; *Schwarzkopf et al.*, 2001] during large sector collapse [*Legros et al.*, 2000], and along caldera-subsidence faults [*Spray*, 1997; *Kokelaar*, 2007]. Future efforts to further constrain fault slip characteristics will afford a better description of volcanic processes, ranging from conduit dynamics to edifice stability and friction-based flow processes, thus contributing to a more accurate assessment of hazards during volcanic crises.

5. Conclusion

Fault friction processes regulating the 1994–95 spine growth, during the 1991–1995 dome eruption at Mt. Unzen, have been investigated using combined seismic analysis and experimental simulations. The seismic record shows the occurrence of clusters of recurring waveforms, revealing a repetitive, cyclic seismic source. These low frequency earthquakes are interpreted to represent repeated faulting events associated with ascent of a plug and extrusion of a lava spine.

Low- to high-velocity rotary shear (HVR) experiments were conducted on Mt. Unzen dacite to constrain the mechanics of fault friction and the character of the slip zone. The experiments show that at mean power densities $<0.3\,\mathrm{MW\,m^{-2}}$, friction takes place along a rock-on-rock slip interface, inducing cataclasis along the fault. Beyond this mean power density threshold, frictional melt forms along the slip interface and temperature dissipation causes viscous remobilization surrounding the fault zone. Close examination of the experimentally generated frictional melt (cooled to pseudotachylyte) indicates a disequilibrium melting process that delivers an unstable shear stress evolution. Subsequent slip ultimately homogenizes the chemistry of the frictional melt, which then exerts a viscous control on the slip zone, which is both normal stress and slip rate dependent. Application of our findings to Mt. Unzen spine growth suggests that during average faulting events at depths below 500 m in the conduit frictional melt may form and act as a viscous brake. At depths below 270 m, viscous remobilization is likely in the glass-bearing host rock, whereas at shallower depths, the cataclastic production of gouge material may lubricate the slip zone. These conflicting effects may limit the propensity of magma to achieve steady state slip conditions during ascent, thereby regulating the seismogenic process of dome growth.

Acknowledgments
We would like to thank H. Mukoyoshi and M. Kitamura for technical assistance at the Kochi Core Centre, and Dirk Müller for assistance with electron microprobe measurements in Munich. We wish to acknowledge the European Research Council (ERC) Starting Grant "SLiM" (Strain localization in magmas, project 306488) and funding provided by the European Union's 7th program for research, technological development, and demonstration under grant agreement 282759 (VUELCO). Kai-Uwe Hess acknowledges the Deutsche Forschungsgemeinschaft, grant HE4565-1 and German Research Foundation (DFG), grant 03G0584A. D.B. Dingwell acknowledges a research professorship from the Bundesexzellenzinitiative (LMUexcellent) and the ERC Advanced Grant "EVOKES" (Explosive volcanism in the earth system: experimental insights, project 247076). We thank John Spray and an anonymous reviewer for constructive reviews of this manuscript. All data not included within tables and figures within the manuscript are held at the corresponding author's institution and are available by request to the corresponding author at a.hornby@liverpool.ac.uk.

References

Alidibirov, M., and D. B. Dingwell (1996), Magma fragmentation by rapid decompression, *Nature*, *380*(6570), 146–148, doi:10.1038/380146a0.

Almberg, L. D., J. F. Larsen, J. C. Eichelberger, T. A. Vogel, and L. C. Patino (2008), Comparison of eruptive and intrusive samples from Unzen Volcano, Japan: Effects of contrasting pressure–temperature–time paths, *J. Volcanol. Geotherm. Res.*, *175*(1–2), 60–70, doi:10.1016/j.jvolgeores.2008.03.020.

Bean, C. J., L. De Barros, I. Lokmer, J.-P. Métaxian, G. O'Brien, and S. Murphy (2013), Long-period seismicity in the shallow volcanic edifice formed from slow-rupture earthquakes, *Nat. Geosci.*, *7*(1), 71–75, doi:10.1038/ngeo2027.

Beeler, N. M., T. E. Tullis, and D. L. Goldsby (2008), Constitutive relationships and physical basis of fault strength due to flash heating, *J. Geophys. Res.*, *113*, B01401, doi:10.1029/2007JB004988.

Benson, P. M., S. Vinciguerra, P. G. Meredith, and R. P. Young (2008), Laboratory simulation of volcano seismicity, *Science*, *322*(5899), 249–252, doi:10.1126/science.1161927.

Bizzarri, A. (2014), The destiny of a clast within a molten pseudotachylyte vein, *Bull. Seismol. Soc. Am.*, *104*(5), 2399–2411, doi:10.1785/0120140084.

Bowden, F. P., and P. A. Persson (1961), Deformation, heating and melting of solids in high-speed friction, *Proc. R. Soc. A*, *260*(1303), 433–458, doi:10.1098/rspa.1961.0044.

Brown, K. M., and Y. Fialko (2012), "Melt welt" mechanism of extreme weakening of gabbro at seismic slip rates, *Nature*, *488*(7413), 638–641, doi:10.1038/nature11370.

Burlini, L., S. Vinciguerra, G. Di Toro, G. De Natale, P. Meredith, and J. P. Burg (2007), Seismicity preceding volcanic eruptions: New experimental insights, *Geology*, *35*(2), 183–186, doi:10.1130/G23195A.1.

Buurman, H., and M. E. West (2010), Seismic precursors to volcanic explosions during the 2006 eruption of Augustine Volcano, in *The 2006 Eruption of Augustine Volcano, Alaska*, edited by J. A. Power, M. L. Coombs, and J. T. Freymueller, *U.S. Geol. Surv. Prof. Pap.*, *1769*, 41–57.

Byerlee, J. (1978), Friction of rocks, *Pure Appl. Geophys.*, *116*, 615–626.

Caricchi, L., L. Burlini, P. Ulmer, T. Gerya, M. Vassalli, and P. Papale (2007), Non-Newtonian rheology of crystal-bearing magmas and implications for magma ascent dynamics, *Earth Planet. Sci. Lett.*, *264*(3–4), 402–419, doi:10.1016/j.epsl.2007.09.032.

Carlslaw, H. S., and J. C. Jaeger (1959), *Conduction of Heat in Solids*, 2nd ed., Oxford Univ. Press, New York.

Chang, J. C., D. A. Lockner, and Z. Reches (2012), Rapid acceleration leads to rapid weakening in earthquake-like laboratory experiments, *Science*, *338*(6103), 101–5, doi:10.1126/science.1221195.

Cashman, K. V., C. R. Thornber, and J. S. Pallister (2008), From dome to dust: Shallow crystallization and fragmentation of conduit magma during the 2004–2006 dome extrusion of Mount St. Helens, Washington, in *A Volcano Rekindled: The First Year of Renewed Eruptions at Mount St. Helens, 2004–2006*, edited by D. R. Sherrod, W. E. Scott, and P. H. Stauffer, *U.S. Geol. Surv. Prof. Pap.*, *1750*.

Chouet, B. (1988), Resonance of a fluid-driven crack: Radiation properties and implications for the source of long-period events and harmonic tremor, *J. Geophys. Res.*, *93*(B5), 4375–4400, doi:10.1029/JB093iB05p04375.

Chouet, B. A., and R. S. Matoza (2013), A multi-decadal view of seismic methods for detecting precursors of magma movement and eruption, *J. Volcanol. Geotherm. Res.*, *252*, 108–175, doi:10.1016/j.jvolgeores.2012.11.013.

Cichy, S. B., R. E. Botcharnikov, F. Holtz, and H. Behrens (2010), Vesiculation and microlite crystallization induced by decompression: A case study of the 1991–1995 Mt Unzen Eruption [Japan], *J. Petrol.*, *52*(7–8), 1469–1492, doi:10.1093/petrology/egq072.

Cimarelli, C., A. Costa, S. Mueller, and H. M. Mader (2011), Rheology of magmas with bimodal crystal size and shape distributions: Insights from analog experiments, *Geochem. Geophys. Geosyst.*, *12*, Q07024, doi:10.1029/2011GC003606.

Collinson, A. S. D., and J. W. Neuberg (2012), Gas storage, transport and pressure changes in an evolving permeable volcanic edifice, *J. Volcanol. Geotherm. Res.*, *243–244*, 1–13, doi:10.1016/j.jvolgeores.2012.06.027.

Cordonnier, B., K.-U. Hess, Y. Lavallée, and D. B. Dingwell (2009), Rheological properties of dome lavas: Case study of Unzen volcano, *Earth Planet. Sci. Lett.*, *279*(3–4), 263–272, doi:10.1016/j.epsl.2009.01.014.

Cordonnier, B., L. Caricchi, M. Pistone, J. Castro, K.-U. Hess, S. Gottschaller, M. Manga, D. B. Dingwell, and L. Burlini (2012a), The viscous-brittle transition of crystal-bearing silicic melt: Direct observation of magma rupture and healing, *Geology*, *40*(7), 611–614, doi:10.1130/G3914.1.

Cordonnier, B., S. M. Schmalholz, K.-U. Hess, and D. B. Dingwell (2012b), Viscous heating in silicate melts: An experimental and numerical comparison, *J. Geophys. Res.*, *117*, B02203, doi:10.1029/2010JB007982.

Costa, A., O. Melnik, and R. S. J. Sparks (2007), Controls of conduit geometry and wallrock elasticity on lava dome eruptions, *Earth Planet. Sci. Lett.*, *260*(1–2), 137–151, doi:10.1016/j.epsl.2007.05.024.

Costa, A., L. Caricchi, and N. Bagdassarov (2009), A model for the rheology of particle-bearing suspensions and partially molten rocks, *Geochem. Geophys. Geosyst.*, *10*, Q03010, doi:10.1029/2008GC002138.

Costa, A., G. Wadge, and O. Melnik (2012), Cyclic extrusion of a lava dome based on a stick–slip mechanism, *Earth Planet. Sci. Lett.*, *337–338*, 39–46, doi:10.1016/j.epsl.2012.05.011.

Costa, A., G. Wadge, R. Stewart, and H. Odbert (2013), Coupled subdaily and multiweek cycles during the lava dome eruption of Soufrière Hills Volcano, Montserrat, *J. Geophys. Res. Solid Earth*, *118*, 1895–1903, doi:10.1002/jgrb.50095.

De Angelis, S., and S. M. Henton (2011), On the feasibility of magma fracture within volcanic conduits: Constraints from earthquake data and empirical modelling of magma viscosity, *Geophys. Res. Lett.*, *38*, L19310, doi:10.1029/2011GL049297.

Dieterich, J. H. (1978), Time-dependent friction and the mechanics of stick-slip, *Pure Appl. Geophys.*, *116*(4-5), 790–806, doi:10.1007/BF00876539.

Dieterich, J. H., and B. D. Kilgore (1994), Direct observation of frictional contacts: New insights for state-dependent properties, *Pure Appl. Geophys.*, *143*(1-3), 283–302, doi:10.1007/BF00874332.

Di Toro, G., T. Hirose, S. Nielsen, G. Pennacchioni, and T. Shimamoto (2006a), Natural and experimental evidence of melt lubrication of faults during earthquakes, *Science*, *311*(5761), 647–649, doi:10.1126/science.1121012.

Di Toro, G., T. Hirose, S. Nielsen, and T. Shimamoto (2006b), in *Earthquakes: Radiated Energy and the Physics of Faulting*, *Geophys. Monogr. Ser.*, edited by R. Abercrombie et al., AGU, Washington, D. C.

Di Toro, G., R. Han, T. Hirose, N. De Paola, S. Nielsen, K. Mizoguchi, F. Ferri, M. Cocco, and T. Shimamoto (2011), Fault lubrication during earthquakes, *Nature*, *471*(7339), 494–498, doi:10.1038/nature09838.

Dingwell, D. B. (1996), Volcanic dilemma—Flow or blow?, *Science*, *273*(5278), 1054–1055, doi:10.1126/science.273.5278.1054.

Dingwell, D. B., C. Romano, and K.-U. Hess (1996), The effect of water on the viscosity of a haplogranitic melt under P-T-X conditions relevant to silicic volcanism, *Contrib. Mineral. Petrol.*, *124*(1), 19–28, doi:10.1007/s004100050170.

Faulkner, D. R., T. M. Mitchell, J. Behnsen, T. Hirose, and T. Shimamoto (2011), Stuck in the mud? Earthquake nucleation and propagation through accretionary forearcs, *Geophys. Res. Lett.*, *38*, L18303, doi:10.1029/2011GL048552.

Fialko, Y. (2004), Temperature fields generated by the elastodynamic propagation of shear cracks in the Earth, *J. Geophys. Res.*, *109*, B01303, doi:10.1029/2003JB002497.

Fialko, Y., and Y. Khazan (2005), Fusion by earthquake fault friction: Stick or slip?, *J. Geophys. Res.*, *110*, B12407, doi:10.1029/2005JB003869.
Giordano, D., J. K. Russell, and D. B. Dingwell (2008), Viscosity of magmatic liquids: A model, *Earth Planet. Sci. Lett.*, *271*(1–4), 123–134, doi:10.1016/j.epsl.2008.03.038.
Goldsby, D. L., and T. E. Tullis (2011), Flash heating leads to low frictional strength of crustal rocks at earthquake slip rates, *Science*, *334*(6053), 216–218, doi:10.1126/science.1207902.
Gonnermann, H., and M. Manga (2003), Explosive volcanism may not be an inevitable consequence of magma fragmentation, *Nature*, *426*(November), 432–435, doi:10.1038/nature02138.
Goto, A. (1999), A new model for volcanic earthquake at Unzen Volcano: Melt rupture model, *Geophys. Res. Lett.*, *26*(16), 2541–2544, doi:10.1029/1999GL900569.
Goto, Y., S. Nakada, M. Kurokawa, T. Shimano, T. Sugimoto, S. Sakuma, H. Hoshizumi, M. Yoshimoto, and K. Uto (2008), Character and origin of lithofacies in the conduit of Unzen volcano, Japan, *J. Volcanol. Geotherm. Res.*, *175*(1–2), 45–59, doi:10.1016/j.jvolgeores.2008.03.041.
Gottsmann, J., and D. B. Dingwell (2001), Cooling dynamics of spatter-fed phonolite obsidian flows on Tenerife, Canary Islands, *J. Volcanol. Geotherm. Res.*, *105*, 323–342, doi:10.1016/S0377-0273(00)00262-6.
Grunewald, U., R. S. J. Sparks, S. Kearns, and J. C. Komorowski (2000), Friction marks on blocks from pyroclastic flows at the Soufriere Hills volcano, Montserrat: Implications for flow mechanisms, *Geology*, *28*(9), 827, doi:10.1130/0091-7613.
Hale, A. J., and G. Wadge (2008), The transition from endogenous to exogenous growth of lava domes with the development of shear bands, *J. Volcanol. Geotherm. Res.*, *171*(3–4), 237–257, doi:10.1016/j.jvolgeores.2007.12.016.
Harrington, R. M., and E. E. Brodsky (2007), Volcanic hybrid earthquakes that are brittle-failure events, *Geophys. Res. Lett.*, *34*, L06308, doi:10.1029/2006GL028714.
Harris, A., W. Rose, and L. Flynn (2003), Temporal trends in lava dome extrusion at Santiaguito 1922–2000, *Bull. Volcanol.*, *1973*, 77–89, doi:10.1007/s00445-002-0243-0.
Hendrasto, M., T. Eto, F. Kimata, T. Matsushima, and K. Ishihara (1997), Magma transport at Mt. Unzen associated with the 1990–1995 activity inferred from levelling data, *Annu. Disaster Prev. Res. Inst., Kyoto Univ.*, *40*(B-1), 61–72.
Hess, K.-U., and D. B. Dingwell (1996), Viscosities of hydrous leucogranitic melts: A non-Arrhenian model, *Am. Mineral.*, *81*, 1297–1300.
Hess, K.-U., D. B. Dingwell, and S. L. Webb (1996a), The influence of alkaline-earth oxides (BeO, MgO, CaO, SrO, BaO) on the viscosity of a haplogranitic melt: Systematics of non-Arrhenian behaviour, *Eur. J. Mineral.*, *8*(3), 371–381.
Hess, K.-U., D. B. Dingwell, and E. Rössler (1996b), Parametrization of viscosity-temperature relations of aluminosilicate melts, *Chem. Geol.*, *128*(1–4), 155–163.
Hirose, T., and T. Shimamoto (2003), Fractal dimension of molten surfaces as a possible parameter to infer the slip-weakening distance of faults from natural pseudotachylytes, *J. Struct. Geol.*, *25*(10), 1569–1574, doi:10.1016/S0191-8141(03)00009-9.
Hirose, T., and T. Shimamoto (2005), Growth of molten zone as a mechanism of slip weakening of simulated faults in gabbro during frictional melting, *J. Geophys. Res.*, *110*, B05202, doi:10.1029/2004JB003207.
Hirose, T., K. Mizoguchi, and T. Shimamoto (2012), Wear processes in rocks at slow to high slip rates, *J. Struct. Geol.*, *38*, 102–116, doi:10.1016/j.jsg.2011.12.007.
Iverson, R. M., et al. (2006), Dynamics of seismogenic volcanic extrusion at Mount St Helens in 2004–05, *Nature*, *444*(7118), 439–443, doi:10.1038/nature05322.
Japanese Meteorological Association (1995), Geological report of eruption at Unzen during a period from November 1994 to February 1995. [Available at http://www.data.jma.go.jp/svd/vois/data/tokyo/STOCK/kaisetsu/CCPVE/Report/061/kaiho_061_18.pdf.]
Johnson, J. B., J. M. Lees, A. Gerst, D. Sahagian, and N. Varley (2008), Long-period earthquakes and co-eruptive dome inflation seen with particle image velocimetry, *Nature*, *456*(7220), 377–381, doi:10.1038/nature07429.
Johnson, J. B., J. J. Lyons, B. J. Andrews, and J. M. Lees (2014), Explosive dome eruptions modulated by periodic gas-driven inflation, *Geophys. Res. Lett.*, *41*, 6689–6697, doi:10.1002/2014GL061310.
Kendrick, J. E., Y. Lavallée, A. Ferk, D. Perugini, R. Leonhardt, and D. B. Dingwell (2012), Extreme frictional processes in the volcanic conduit of Mount St. Helens (USA) during the 2004–2008 eruption, *J. Struct. Geol.*, *38*, 61–76, doi:10.1016/j.jsg.2011.10.003.
Kendrick, J. E., Y. Lavallée, T. Hirose, G. Di Toro, A. J. Hornby, S. De Angelis, and D. B. Dingwell (2014a), Volcanic drumbeat seismicity caused by stick–slip motion and magmatic frictional melting, *Nat. Geosci.*, *7*(June), 438–442, doi:10.1038/ngeo2146.
Kendrick, J. E., Y. Lavallée, K.-U. Hess, S. De Angelis, A. Ferk, H. E. Gaunt, P. G. Meredith, D. B. Dingwell, and R. Leonhardt (2014b), Seismogenic frictional melting in the magmatic column, *Solid Earth*, *5*, 199–208, doi:10.5194/se-5-199-2014.
Kennedy, L. A., and J. K. Russell (2012), Cataclastic production of volcanic ash at Mount Saint Helens, *Phys. Chem. Earth, Parts A/B/C*, *45–46*, 40–49, doi:10.1016/j.pce.2011.07.052.
Kennedy, L. A., J. K. Russell, and E. Nelles (2009), Origins of Mount St. Helens cataclasites: Experimental insights, *Am. Mineral.*, *94*(7), 995–1004, doi:10.2138/am.2009.3129.
Ketner, D., and J. Power (2013), Characterization of seismic events during the 2009 eruption of Redoubt Volcano, Alaska, *J. Volcanol. Geotherm. Res.*, *259*, 45–62, doi:10.1016/j.jvolgeores.2012.10.007.
Kohno, Y., T. Matsushima, and H. Shimizu (2008), Pressure sources beneath Unzen Volcano inferred from leveling and GPS data, *J. Volcanol. Geotherm. Res.*, *175*(1–2), 100–109, doi:10.1016/j.jvolgeores.2008.03.022.
Koizumi, Y., K. Otsuki, A. Takeuchi, and H. Nagahama (2004), Frictional melting can terminate seismic slips: Experimental results of stick-slips, *Geophys. Res. Lett.*, *31*, L21605, doi:10.1029/2004GL020642.
Kokelaar, P. (2007), Friction melting, catastrophic dilation and breccia formation along caldera superfaults, *J. Geol. Soc. London*, *164*, 751–754.
Kolzenburg, S., and J. K. Russell (2014), Welding of pyroclastic conduit infill: A mechanism for cyclical explosive eruptions, *J. Geophys. Res. Solid Earth*, *119*, 5305–5323, doi:10.1002/2013JB010931.
Kusakabe, M., H. Sato, S. Nakada, and T. Kitamura (1999), Water contents and hydrogen isotopic ratios of rocks and minerals from the 1991 eruption of Unzen volcano, Japan, *J. Volcanol. Geotherm. Res.*, *89*, 231–242.
Lamb, O. D., N. R. Varley, T. A. Mather, D. M. Pyle, P. J. Smith, and E. J. Liu (2014), Similar cyclic behaviour observed at two lava domes, Volcán de Colima (Mexico) and Soufrière Hills volcano (Montserrat), with implications for monitoring, *J. Volcanol. Geotherm. Res.*, *284*, 106–121, doi:10.1016/j.jvolgeores.2014.07.013.
Lavallée, Y., K.-U. Hess, B. Cordonnier, and D. Bruce Dingwell (2007), Non-Newtonian rheological law for highly crystalline dome lavas, *Geology*, *35*(9), 843, doi:10.1130/G23594A.1.
Lavallée, Y., P. G. Meredith, D. B. Dingwell, K.-U. Hess, J. Wassermann, B. Cordonnier, A. Gerik, and J. H. Kruhl (2008), Seismogenic lavas and explosive eruption forecasting, *Nature*, *453*(7194), 507–510, doi:10.1038/nature06980.
Lavallée, Y., P. M. Benson, M. J. Heap, A. Flaws, K.-U. Hess, and D. B. Dingwell (2011), Volcanic conduit failure as a trigger to magma fragmentation, *Bull. Volcanol.*, *74*(1), 11–13, doi:10.1007/s00445-011-0544-2.

Lavallée, Y., T. M. Mitchell, M. J. Heap, J. Vasseur, K.-U. Hess, T. Hirose, and D. B. Dingwell (2012), Experimental generation of volcanic pseudotachylytes: Constraining rheology, *J. Struct. Geol.*, *38*, 222–233, doi:10.1016/j.jsg.2012.02.001.
Lavallée, Y., P. M. Benson, M. J. Heap, K.-U. Hess, A. Flaws, B. Schillinger, P. G. Meredith, and D. B. Dingwell (2013), Reconstructing magma failure and the degassing network of dome-building eruptions, *Geology*, *41*(4), 515–518, doi:10.1130/G33948.1.
Lavallée, Y., T. Hirose, J. E. Kendrick, S. De Angelis, L. Petrakova, A. J. Hornby, and D. B. Dingwell (2014), A frictional law for volcanic ash gouge, *Earth Planet. Sci. Lett.*, *400*, 177–183, doi:10.1016/j.epsl.2014.05.023.
Lavallée, Y., M. J. Heap, U. Kueppers, J. E. Kendrick, and D. B. Dingwell (2016), The fragility of Volcán de Colima—A material constraint, in *Volcán de Colima–Managing the Threat*, edited by N. R. Varley and J.-C. Komorowski, Springer, Berlin, in press.
Legros, F., J. Cantagrel, and B. Devouard (2000), Pseudotachylyte (Frictionite) at the Base of the Arequipa Volcanic Landslide Deposit (Peru): Implications for Emplacement Mechanisms, *J. Geol.*, *108*, 601–611, doi:10.1086/314421.
Lejeune, A. M., Y. Bottinga, T. W. Trull, and P. Richet (1999), Rheology of bubble-bearing magmas, *Earth Planet. Sci. Lett.*, *166*(1–2), 71–84, doi:10.1016/S0012-821X(98)00278-7.
Lensky, N., R. Sparks, O. Navon, and V. Lyakhovsky (2008), Cyclic activity at Soufrière Hills Volcano, Montserrat: Degassing-induced pressurization and stick–slip extrusion, *Geol. Soc. London Spec. Publ.*, *307*, 169–188.
Lyons, J. J., G. P. Waite, M. Ichihara, and J. M. Lees (2012), Tilt prior to explosions and the effect of topography on ultra-long-period seismic records at Fuego volcano, Guatemala, *Geophys. Res. Lett.*, *39*, L08305, doi:10.1029/2012GL051184.
Mader, H. M., E. W. Llewellin, and S. P. Mueller (2013), The rheology of two-phase magmas: A review and analysis, *J. Volcanol. Geotherm. Res.*, *257*, 135–158, doi:10.1016/j.jvolgeores.2013.02.014.
Maryanto, S., M. Iguchi, and T. Tameguri (2008), Constraints on the source mechanism of harmonic tremors based on seismological, ground deformation, and visual observations at Sakurajima volcano, Japan, *J. Volcanol. Geotherm. Res.*, *170*(3–4), 198–217, doi:10.1016/j.jvolgeores.2007.10.004.
Massol, H., and C. Jaupart (2009), Dynamics of magma flow near the vent: Implications for dome eruptions, *Earth Planet. Sci. Lett.*, *279*(3–4), 185–196, doi:10.1016/j.epsl.2008.12.041.
Michaut, C., Y. Ricard, D. Bercovici, and R. S. J. Sparks (2013), Eruption cyclicity at silicic volcanoes potentially caused by magmatic gas waves, *Nat. Geosci.*, *6*(10), 856–860, doi:10.1038/ngeo1928.
Mizoguchi, K., T. Hirose, T. Shimamoto, and E. Fukuyama (2009), High-velocity frictional behavior and microstructure evolution of fault gouge obtained from Nojima fault, southwest Japan, *Tectonophysics*, *471*(3–4), 285–296, doi:10.1016/j.tecto.2009.02.033.
Moore, P. L., N. R. Iverson, and R. M. Iverson (2008), Frictional properties of the Mount St. Helens gouge, in *A Volcano Rekindled: The First Year of Renewed Eruptions at Mount St. Helens, 2004–2006*, edited by D. R. Sherrod, W. E. Scott, and P. H. Stauffer, *U.S. Geol. Surv. Prof. Pap.*, *1750*.
Mueller, S., E. W. Llewellin, and H. M. Mader (2011), The effect of particle shape on suspension viscosity and implications for magmatic flows, *Geophys. Res. Lett.*, *38*, L13316, doi:10.1029/2011GL047167.
Nakada, S., and Y. Motomura (1999), Petrology of the 1991–1995 eruption at Unzen: Effusion pulsation and groundmass crystallization, *J. Volcanol. Geotherm. Res.*, *89*(1–4), 173–196, doi:10.1016/S0377-0273(98)00131-0.
Nakada, S., H. Shimizu, and K. Ohta (1999), Overview of the 1990–1995 eruption at Unzen Volcano, *J. Volcanol. Geotherm. Res.*, *89*(1–4), 1–22, doi:10.1016/S0377-0273(98)00118-8.
Neuberg, J. W., H. Tuffen, L. Collier, D. Green, T. Powell, and D. Dingwell (2006), The trigger mechanism of low-frequency earthquakes on Montserrat, *J. Volcanol. Geotherm. Res.*, *153*(1–2), 37–50, doi:10.1016/j.jvolgeores.2005.08.008.
Nielsen, S., G. Di Toro, T. Hirose, and T. Shimamoto (2008), Frictional melt and seismic slip, *J. Geophys. Res.*, *113*, B01308, doi:10.1029/2007JB005122.
Nishimura, K., T. Kawamoto, T. Kobayashi, T. Sugimoto, and S. Yamashita (2005), Melt inclusion analysis of the Unzen 1991–1995 dacite: Implications for crystallization processes of dacite magma, *Bull. Volcanol.*, *67*(7), 648–662, doi:10.1007/s00445-004-0400-8.
Noguchi, S., A. Toramaru, and S. Nakada (2008), Relation between microlite textures and discharge rate during the 1991–1995 eruptions at Unzen, Japan, *J. Volcanol. Geotherm. Res.*, *175*(1–2), 141–155, doi:10.1016/j.jvolgeores.2008.03.025.
Ohtomo, Y., and T. Shimamoto (1994), Significance of thermal fracturing in the generation of fault gouge during rapid fault motion: An experimental verification, *J. Tectonic Res. Group Jpn.*, *39*, 135–144.
Okumura, S., M. Nakamura, T. Nakano, K. Uesugi, and A. Tsuchiyama (2010), Shear deformation experiments on vesicular rhyolite: Implications for brittle fracturing, degassing, and compaction of magmas in volcanic conduits, *J. Geophys. Res.*, *115*, B06201, doi:10.1029/2009JB006904.
Okumura, S., M. Nakamura, K. Uesugi, T. Nakano, and T. Fujioka (2013), Coupled effect of magma degassing and rheology on silicic volcanism, *Earth Planet. Sci. Lett.*, *362*, 163–170, doi:10.1016/j.epsl.2012.11.056.
Pallister, J. S., K. V. Cashman, J. T. Hagstrum, N. M. Beeler, S. C. Moran, and R. P. Denlinger (2013), Faulting within the Mount St. Helens conduit and implications for volcanic earthquakes, *Geol. Soc. Am. Bull.*, *125*(3–4), 359–376, doi:10.1130/B30716.1.
Plail, M., M. Edmonds, M. C. S. Humphreys, J. Barclay, and R. A. Herd (2014), Geochemical evidence for relict degassing pathways preserved in andesite, *Earth Planet. Sci. Lett.*, *386*, 21–33, doi:10.1016/j.epsl.2013.10.044.
Reyes, C. G., and M. E. West (2011), The waveform suite: A robust platform for manipulating waveforms in MATLAB, *Seismol. Res. Lett.*, *82*(1), 104–110, doi:10.1785/gssrl.
Ruina, A. (1983), Slip instability and state variable friction laws, *J. Geophys. Res.*, *88*, 10,359, doi:10.1029/JB088iB12p10359.
Rust, A. C., K. V. Cashman, and P. J. Wallace (2004), Magma degassing buffered by vapor flow through brecciated conduit margins, *Geology*, *32*(4), 349–352, doi:10.1130/G20388.2.
Saito, T., and N. Ishikawa (2012), Pre- and syn-eruptive conditions inferred from the magnetic petrology of Fe–Ti oxides from three historical eruptions of Unzen Volcano, Japan, *J. Volcanol. Geotherm. Res.*, *247–248*, 49–61, doi:10.1016/j.jvolgeores.2012.07.013.
Scharff, L., M. Hort, and A. Gerst (2014), The dynamics of the dome at Santiaguito volcano, Guatemala, *Geophys. J. Int.*, doi:10.1093/gji/ggu069.
Schwarzkopf, L., H.-U. Schmincke, and V. Troll (2001), Pseudotachylite on impact marks of block surfaces in block-and-ash flows at Merapi volcano, Central Java, Indonesia, *Int. J. Earth Sci.*, *90*(4), 769–775, doi:10.1007/s005310000171.
Shand, S. J. (1916), The pseudotachylyte of Parijs (Orange Free State), and its relation to "trap-shotten gneiss" and "flinty crush-rock", *Q. J. Geol. Soc.*, *72*, 198–221, doi:10.1144/GSL.JGS.1916.072.01-04.12.
Sheorey, P. R. (1994), A theory for in situ stresses in isotropic and transversely isotropic rock, *Int. J. Rock Mech. Min. Sci. Geomech. Abstr.*, *31*(1), 23–34, doi:10.1016/0148-9062(94)91070-7.
Shimamoto, T., and A. Lin (1994), Is frictional melting equilibrium melting, or non-equilibrium melting?, *J. Tectonic Res. Group Jpn.*, *39*, 79–84.
Shimamoto, T., and A. Tsutsumi (1994), A new rotary-shear high-speed frictional testing machine: Its basic design and scope of research, *J. Tectonic Res. Group Jpn.*, *39*, 65–78.

Sibson, R. (1975), Generation of pseudotachylyte by ancient seismic faulting, *Geophys. J. Int.*, *43*(3), 775–794, doi:10.1111/j.1365-246X.1975.tb06195.x.

Smith, J. V., Y. Miyake, and T. Oikawa (2001), Interpretation of porosity in dacite lava domes as ductile–brittle failure textures, *J. Volcanol. Geotherm. Res.*, *112*(1–4), 25–35, doi:10.1016/S0377-0273(01)00232-3.

Sone, H., and T. Shimamoto (2009), Frictional resistance of faults during accelerating and decelerating earthquake slip, *Nat. Geosci.*, doi:10.1038/ngeo637.

Sparks, R. S. J. (2000), The causes and consequences of eruptions of andesite volcanoes: Opening remarks, *Philos. Trans. R. Soc. London, Ser. A*, *358*(1770), 1435–1440, doi:10.1098/rsta.2000.0596.

Spray, J. G. (1997), Superfaults, *Geology*, *25*(7), 579–582.

Spieler, O., B. Kennedy, U. Kueppers, D. B. Dingwell, B. Scheu, and J. Taddeucci (2004), The fragmentation threshold of pyroclastic rocks, *Earth Planet. Sci. Lett.*, *226*(1–2), 139–148, doi:10.1016/j.epsl.2004.07.016.

Spray, J. G. (1992), A physical basis for the frictional melting of some rock-forming minerals, *Tectonophysics*, *204*(3–4), 205–221, doi:10.1016/0040-1951(92)90308-S.

Spray, J. G. (1993), Viscosity determinations of some frictionally generated silicate melts: Implications for fault zone rheology at high strain rates, *J. Geophys. Res.*, *98*(B5), 8053–8068, doi:10.1029/93JB00020.

Spray, J. G. (2005), Evidence for melt lubrication during large earthquakes, *Geophys. Res. Lett.*, *32*, L07301, doi:10.1029/2004GL022293.

Spray, J. G. (2010), Frictional melting processes in planetary materials: From hypervelocity impact to earthquakes, *Annu. Rev. Earth Planet. Sci.*, *38*(1), 221–254, doi:10.1146/annurev.earth.031208.100045.

Thomas, M. E., and J. Neuberg (2012), What makes a volcano tick—A first explanation of deep multiple seismic sources in ascending magma, *Geology*, *40*(4), 351–354, doi:10.1130/G32868.1.

Truby, J. M., S. P. Mueller, E. W. Llewellin, and H. M. Mader (2015), The rheology of three-phase suspensions at low bubble capillary number, *Proc. Math. Phys. Eng. Sci.*, *471*(2173), 20140557, doi:10.1098/rspa.2014.0557.

Tsutsumi, A., and T. Shimamoto (1997), Temperature measurements along simulated faults during seismic fault motion, Proc. 30th, *Int. Geol. Congr.*, *5*, 223–232.

Tuffen, H., and D. Dingwell (2004), Fault textures in volcanic conduits: Evidence for seismic trigger mechanisms during silicic eruptions, *Bull. Volcanol.*, *67*(4), 370–387, doi:10.1007/s00445-004-0383-5.

Uhira, K., H. Yamasato, T. Hashimoto, K. Fukui, and M. Takeo (1995), Source mechanism of low-frequency seismic events at Unzen Volcano, Kyushu, Japan, *Bull. Volcanol. Soc. Jpn.*, *40*(5), 311–328.

Umakoshi, K., N. Takamura, N. Shinzato, K. Uchida, N. Matsuwo, and H. Shimizu (2008), Seismicity associated with the 1991–1995 dome growth at Unzen Volcano, Japan, *J. Volcanol. Geotherm. Res.*, *175*(1–2), 91–99, doi:10.1016/j.jvolgeores.2008.03.030.

Umakoshi, K., N. Itasaka, and H. Shimizu (2011), High-frequency earthquake swarm associated with the May 1991 dome extrusion at Unzen Volcano, Japan, *J. Volcanol. Geotherm. Res.*, *206*(3–4), 70–79, doi:10.1016/j.jvolgeores.2011.07.004.

Varley, N., R. Arámbula-Mendoza, G. Reyes-Dávila, R. Sanderson, and J. Stevenson (2010), Generation of Vulcanian activity and long-period seismicity at Volcán de Colima, Mexico, *J. Volcanol. Geotherm. Res.*, *198*(1–2), 45–56, doi:10.1016/j.jvolgeores.2010.08.009.

Venezky, D. Y., and M. J. Rutherford (1999), Petrology and Fe–Ti oxide reequilibration of the 1991 Mount Unzen mixed magma, *J. Volcanol. Geotherm. Res.*, *89*(1–4), 213–230, doi:10.1016/S0377-0273(98)00133-4.

Violay, M., G. Di Toro, B. Gibert, S. Nielsen, E. Spagnuolo, P. Del Gaudio, P. Azais, and P. G. Scarlato (2014), Effect of glass on the frictional behavior of basalts at seismic slip rates, *Geophys. Res. Lett.*, *41*, 348–355, doi:10.1002/2013GL058601.

Voight, B. (1999), Magma flow instability and cyclic activity at Soufriere Hills volcano, Montserrat, British West Indies, *Science*, *283*(5405), 1138–1142, doi:10.1126/science.283.5405.1138.

Waite, G. P., B. A. Chouet, and P. B. Dawson (2008), Eruption dynamics at Mount St. Helens imaged from broadband seismic waveforms: Interaction of the shallow magmatic and hydrothermal systems, *J. Geophys. Res.*, *113*, B02305, doi:10.1029/2007JB005259.

Watts, R. B., R. A. Herd, R. S. J. Sparks, and S. R. Young (2002), Growth patterns and emplacement of the andesitic lava dome at Soufriere Hills Volcano, Montserrat, *Geol. Soc. London Mem.*, *21*(1), 115–152, doi:10.1144/GSL.MEM.2002.021.01.06.

Webb, S. L., and D. B. Dingwell (1990), Non-Newtonian rheology of igneous melts at high stresses and strain rates: Experimental results for rhyolite, andesite, basalt, and nephelinite, *J. Geophys. Res.*, *95*(B10), 15,695–15,701, doi:10.1029/JB095iB10p15695.

Yamasato, H. (1998), Nature of infrasonic pulse accompanying low frequency earthquake at Unzen Volcano, Japan, *Bull. Volcanol. Soc. Jpn.*, *43*(1), 1–13.

Yamashina, K., T. Matsushima, and S. Ohmi (1999), Volcanic deformation at Unzen, Japan, visualized by a time-differential stereoscopy, *J. Volcanol. Geotherm. Res.*, *89*(1–4), 73–80, doi:10.1016/S0377-0273(98)00124-3.